UC-404
LBL-25741
c.1

Center for Advanced Materials

CAM

RECEIVED
LAWRENCE
BERKELEY LABORATORY
OCT 11 1988
LIBRARY AND
DOCUMENTS SECTION

Tensile and Shear Behavior of Alloyed Sn-Pb Solder Joints

L.K. Quan
(M.S. Thesis)

August 1988

For Reference

Not to be taken from this room

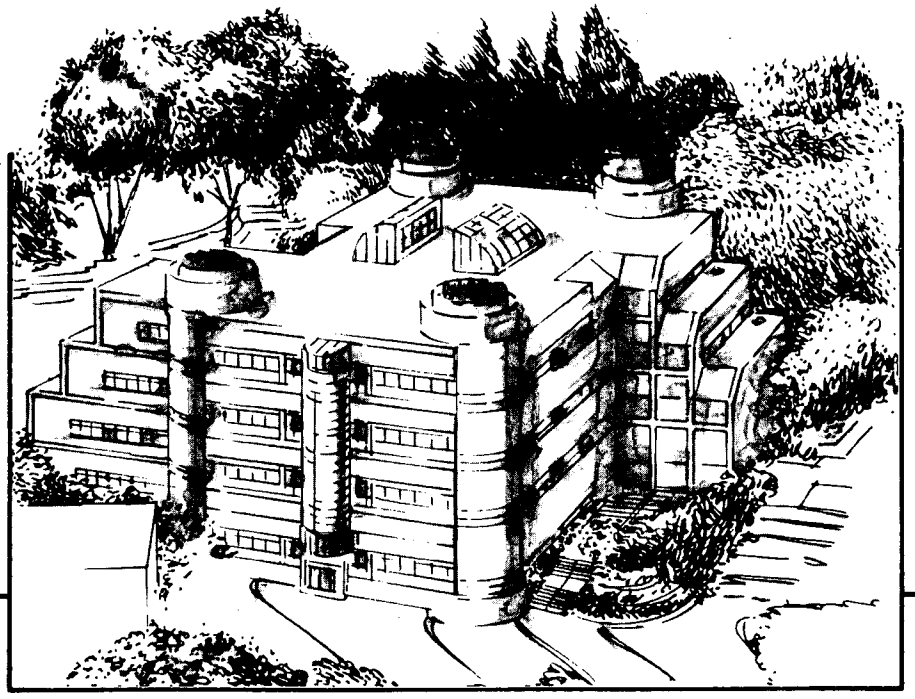

Materials and Chemical Sciences Division

Lawrence Berkeley Laboratory • University of California

ONE CYCLOTRON ROAD, BERKELEY, CA 94720 • (415) 486-4755

Prepared for the U.S. Department of Energy under Contract DE-AC03-76SF00098

LBL-25741
c.1

DISCLAIMER

This document was prepared as an account of work sponsored by the United States Government. While this document is believed to contain correct information, neither the United States Government nor any agency thereof, nor the Regents of the University of California, nor any of their employees, makes any warranty, express or implied, or assumes any legal responsibility for the accuracy, completeness, or usefulness of any information, apparatus, product, or process disclosed, or represents that its use would not infringe privately owned rights. Reference herein to any specific commercial product, process, or service by its trade name, trademark, manufacturer, or otherwise, does not necessarily constitute or imply its endorsement, recommendation, or favoring by the United States Government or any agency thereof, or the Regents of the University of California. The views and opinions of authors expressed herein do not necessarily state or reflect those of the United States Government or any agency thereof or the Regents of the University of California.

LBL 25741

Tensile and Shear Behavior of Alloyed Sn-Pb Solder Joints

L. K. Quan

M.S. Thesis

Center for Advanced Materials
Materials and Chemical Sciences Division
Lawrence Berkeley Laboratory
University of California

and

Department of Materials Science and Mineral Engineering
University of California at Berkeley
Berkeley, California 94720

August 1988

This work is supported by the Director, Office of Energy Research, Office of Fusion Energy, Development and Technology Divison of the U. S. Department of Energy under Contract No. DE-AC03-76SF00098

ACKNOWLEDGMENTS

Special thanks are extended to my research adviser, Prof J.W. Morris Jr., for his guidance and support throughout this project and throughout my academic career. I am also thankful to the members of my thesis committee, Prof R.O. Ritchie and Prof F.E. Hauser, for their review and constructive criticism of this manuscript.

I would like to express my appreciation to Dr. D. Grivas for his guidance in the initiation of this project and especially to D. Tribula for her helpful discussions and review of this thesis.

Finally, I would like to thank my parents for their encouragement, their faith in my abilities, and their many sacrifices in providing me with a choice education which I oftentimes take for granted.

This work was supported by the Director, Office of Energy Research, Office of Basic Energy Science, Material Sciences Division of the U.S. Department of Energy under Control No. DE-ACO3-76SF00098. Financial support was also provided in part by fellowship from Western Digital Corporation.

TABLE OF CONTENTS

1. INTRODUCTION 1
2. EXPERIMENTAL PROCEDURE 3
   2.1 Specimen Preparation 3
   2.2 Mechanical Testing 5
   2.3 Microscopy 5
3. RESULTS 7
   3.1 Microstructure 7
   3.2 Mechanical Properties 9
4. DISCUSSION 10
   4.1 Microstructure 10
   4.2 Mechanical Properties 14
   4.3 Alloy Development 16
5. CONCLUSIONS 18
6. REFERENCES 19
   FIGURES 20

Tensile and Shear Behavior of Alloyed Sn-Pb Solder Joints

L. K. Quan

Center for Advanced Materials, Lawrence Berkeley Laboratory and
Department of Materials Science and Engineering,
University of California, Berkeley

1. INTRODUCTION

Tin-lead solders are used extensively in the electronics industry as a joining material in electronic packaging. Electronic packaging, the housing and interconnection of electronic devices, is divided into a three-tiered hierarchy. In the first level, a silicon die is housed in a plastic or ceramic package. First level interconnections join the contacts on the devices to external leads on the package. In the second level, the packages are integrated on a polymeric printed circuit board (PCB). Eutectic or near-eutectic Sn-Pb solders are used to bond the leads to conductive Cu lines or holes on the board. Finally, in the third level, various boards are mounted on edge on a larger board to complete the system. Tin-lead solders are well suited for packaging applications because of their low melting temperatures (Figure 1); the soldering process can take place at relatively low temperatures, thereby minimizing the risk of heat damage to devices. In addition to the temperature consideration, Sn-Pb base alloys are preferred because of their relatively low price and their adequate wetting and strength properties.[1]

Surface mount technology of leadless chip carriers is emerging as a promising technology for second level packaging.[2-5] In surface mount, package leads are soldered to pads on the surface of the PCB, as opposed to inserting leads through the board and soldering them to the back side as in the conventional plated-through-hole technology.

Leadless chip carriers have the external leads removed and replaced by metallized layers deposited directly on the package; solder joins the metallization on the package to the pad on the board (Figure 2). Used in conjunction, surface mount and leadless chip carriers offer several methods of increasing circuit densities and thus reducing signal delay times. For example, packages can be placed on both sides of the PCB leading to a twofold increase in density. Densities can be increased further since space consuming holes are no longer necessary. Also, package sizes can be reduced since lead pitch, the spacing between adjacent leads, can be reduced.

During the normal operation of a device, thermal excursions are encountered. These thermal excursions may be caused either by Joule heating during the operational on/off cycle or by changes in the ambient temperature. Because the solder joins two materials of different thermal coefficients of expansion, a condition of strain-controlled thermal fatigue is experienced by the solder. This problem is accentuated in surface mounted leadless chip carriers; more severe operating conditions are experienced by the solder since the compliant lead has been removed.

Potential improvements in the properties of the solder can be achieved by altering either the microstructure or the processing history. The microstructure, in turn, can be tailored by altering either the composition of the solder or the processing history. However, since any post-soldering deformation or heat treatment risks damage to devices, processing parameters are limited. This suggests that improvements in the properties of solders be made by modifying the microstructure via a change in composition. To maintain the advantages of the Sn-Pb base system and to introduce only minor modifications to the soldering process, the use of near-eutectic Sn-Pb-X ternary alloys is desirable.

Limited data is available on the effects of ternary additions to the Sn-Pb system. Most of the published literature addresses production concerns and considers the effects of contamination additions on the wetting characteristics and the physical appearance of

the joint.[6] Few accompanying microstructural observations or mechanical properties with well defined experimental conditions are available.

Before an extensive alloy development program is initiated, a fundamental study of the effects of ternary additions to the Sn-Pb base solder system is necessary for the selection of alloys for further study. This study presents an investigation of three ternary additions to a near-eutectic Sn-Pb alloy: indium (In), bismuth (Bi), and antimony (Sb). The effects of these ternary additions on the microstructure and on the strength in tensile and shear loading conditions in a joint configuration were studied.

2. EXPERIMENTAL PROCEDURE

2.1 Specimen Preparation

The following solder alloys (weight %) were investigated:

60Sn-40Pb

58Sn-40Pb-2In

58Sn-40Pb-2Bi

58Sn-40Pb-2Sb

Each alloy was tested in a joint configuration soldered to Cu.

Solder alloys were prepared from the following:

Element	Form	% Purity
Sn	brick	99.9
Pb	brick	99.94
In	shot	99.99
Bi	shot	99.995
Sb	bar	99.999

Bulk solder ingots and joint specimens were prepared in the furnace apparatus shown schematically in Figure 3. The apparatus consists of a vacuum chamber which can be backfilled with argon and two heating coils. The lower heating coil is used to melt the solder ingots while the upper heating coil is used to preheat the Cu plates. The temperature at each location is controlled separately.

The Sn and Pb bricks were further refined by segregation after receiving. Each metal was heated to 50°C above its melting temperature, then directionally solidified by immersion of the bottom of the quartz crucible in an ice water bath. After cooling, the top of the ingot was removed and discarded.

Appropriate amounts of the two metals were melted after the initial refining process. The melt was held at 375°C for 15 min. The ingot was then cooled by immersion of the quartz crucible in an ice water bath. After cooling, the ingot was removed, inverted, and the process repeated at a temperature of 240°C to insure mixing of the alloy.

The manufacturing procedure for the tensile and shear specimens is shown schematically in Figures 4 and 5. Cold-rolled 99.9% OFHC Cu sheets of thicknesses 13 mm, 6 mm, and 3 mm were machined to the proper dimensions to manufacture the tensile and shear specimens, respectively. The surfaces to be soldered were polished through 6 μm diamond paste. The Cu plates were etched in 50% HNO_3 for 1 min, then lightly coated with Johnson's stainless steel soft soldering flux to remove and prevent surface oxidation. The Cu plates were assembled with aluminum spacers of various thicknesses inserted to form a gap for the desired solder joint thicknesses. The outer surfaces of the assembly were lightly coated with a refractory paste to prevent wetting for easy removal of the assembly from the solder ingot.

The Cu assembly was hung in the upper furnace of the apparatus shown in Figure 3. The previously prepared solder ingot was placed in the lower furnace. Both Cu and solder were heated to approximately 240°C. After thermal equilibrium was

established, the Cu plates were slowly immersed into the solder bath. Molten solder flowed up the gap to form the solder joint. To prevent the solder from flowing out of the joint, the assembly was left in the solder bath and cooled by immersion of the quartz crucible into an ice water bath.

The solder block containing the Cu specimens was removed from the graphite crucible and excess solder was machined from the specimen. The remaining solder was easily chiseled from the Cu surface. The block was then machined to form the appropriate grooves.

The block was sectioned with a diamond wafering blade on a low speed saw. Each block yielded 8-10 specimens of identical composition and processing history, thereby insuring specimen uniformity within the same batch.

Final machining was done after the specimens were sectioned. The final tensile and shear specimen configurations are shown in Figures 6 and 7.

2.2 Mechanical Testing

Specimen configurations for mechanical testing are shown in Figures 6 and 7. The tensile specimen used was a butt joint specimen with a 1.0 mm joint thickness. The joint thickness was chosen in an attempt to avoid interfacial failures due to joint constraint while still testing a joint microstructure. The shear specimen was a modified double-lap shear specimen. The grooves isolate the solder in the center of the specimen; under a tensile load, the two center solder joints are deformed in shear.[7]

Mechanical testing was performed by straining the specimens to failure at room temperature on a screw-driven mechanical load frame at a crosshead speed 0.05 mm/min. Load-displacement data was recorded on a strip-chart recorder, then converted to engineering stress-strain curves. The gauge length was defined as the solder thickness, assuming the elastic strains in the Cu were negligible. Using this consideration, the corresponding strain rates were 0.05 min^{-1} for both the tensile and shear testing.

[*NB:* The shear strain was defined as $\varepsilon_{ij} = 1/2\ \{(\delta u_i/\delta x_j) + (\delta u_j/\delta x_i)\}$ where u_i was the displacement in the i-direction and x_j was the position in the j-direction.] The reported strength values correspond to the ultimate strengths, each value representing an average of three specimens.

2.3 Microscopy

The joint microstructure of each alloy was examined in the as-soldered condition. After mechanical testing, fracture surfaces were observed by scanning electron microscopy (SEM). Also, the cross-sections of the specimens were repolished and the crack profiles were examined (Figure 8).

Specimens for optical microscopy were prepared as follows. Specimens were ground through 600 grit SiC paper. This was followed by polishing with 1 μm and 0.05 μm Al_2O_3, respectively. Final polishing was done with colloidal silica (Mastermet by Buehler) on microcloth. The microstructure was revealed after the final polish; no subsequent chemical etch was required.

Light microscopy was performed on a Nikon Epiphot-TME. Depth of field was obtained using a differential interference attachment. Scanning electron microscopy was performed on an ISI WB-6 at 25 kV accelerating voltage. An EG&G Ortec System 5000 was used for chemical analysis by energy dispersive spectroscopy (EDS).

3. RESULTS

3.1 Microstructure

<u>60Sn-40Pb:</u> Micrographs of the 60Sn-40Pb tensile joint microstructure are shown in Figure 9. The microstructure consists of proeutectic dendrites of the Pb-rich α-phase and a eutectic mixture of the Pb-rich α-phase and the Sn-rich β-phase,

Figure 9(a). The eutectic microstructure consists of grains with well-defined grain boundaries, Figure 9(b). The structure within each eutectic grain varies from grain to grain; the structure in some grains appears globular while in others the structure is lamellar. Within the lamellar grains, sub-grains or "colonies" can sometimes be distinguished, Figure 9(c).

Two interfacial intermetallics are observed at the solder/Cu interface (Figure 10). These intermetallics were identified by EDS as the Cu_3Sn ε-phase (adjacent to the Cu) and the Cu_6Sn_5 η-phase (adjacent to the solder). The Cu_3Sn forms a thin continuous film while the Cu_6Sn_5 forms in an acicular morphology.

In addition to the interfacial intermetallics, intermetallics are observed within the solder (Figure 11). These bulk intermetallics were identified as Cu_6Sn_5. The Cu_6Sn_5 bulk intermetallics are of a hexagonal rod-like morphology. Typically, the rods are "hollow" and the central core is filled with solder.

TERNARY ALLOYS: Interfacial and bulk intermetallics are present in the ternary specimens as in the binary specimens. As in the 60Sn-40Pb alloy, the ternary microstructures contain dendrites of the primary α-phase and a eutectic structure of the Pb-rich α-phase and the Sn-rich β-phase. However, the amount of α-dendrites and the morphology of the background eutectic structure varies among the alloys.

The microstructures of the 58Sn-40Pb-2In and 58Sn-40Pb-2Bi tensile specimens are not identical, but general similarities can be found between the two microstructures which can be contrasted with the 60Sn-40Pb microstructure. The amount of primary α in the In and Bi alloyed specimens is similar to the amount present in the 60Sn-40Pb specimen. The eutectic microstructure (Figure 12) consists of grains of α-Pb and β-Sn. The eutectic structure of these alloys is homogeneous; each grain has similar shape and morphology. The morphology of the particles within these grains is either lamellar or globular in the center of the grains; the morphology of the particles at the outer areas of the grains is always globular. The phase particles in the globular grains appear to have

some alignment. Compared to the 60Sn-40Pb alloy, the grains in the In and Bi alloys are small and the grain boundaries are diffuse; the phase particle size gradually coarsens toward the grain boundaries.

The 58Sn-40Pb-2Sb tensile specimen has very few dendrites of primary α. The eutectic structure of the 58Sn-40Pb-2Sb tensile specimen varies throughout the specimen. Most regions resemble the binary alloy having large grains and well defined grain boundaries, Figure 13(a). However, some regions resemble the In and Bi alloyed specimens with small grains and diffuse grain boundaries, Figure 13(b). The phase particle size of the 58Sn-40Pb-2Sb alloy is the finest of the alloys studied.

TENSILE VS. SHEAR: Micrographs of the shear specimens are shown in Figures 14 and 15. Slight variations in the amount of proeutectic α in the tensile and shear specimens exist. However, in general, the microstructures of the shear specimens are coarser, although qualitatively similar to their tensile counterparts.

The In-containing shear specimen has fewer dendrites of proeutectic α than the In-containing tensile specimen. On the other hand, the Bi-containing shear specimen has more proeutectic α than the corresponding tensile specimen. For both alloys, however, the eutectic structure appears similar in the tensile and shear configurations.

The 58Sn-40Pb-2Sb shear specimen microstructure is noticeably different from the microstructure in the tensile configuration. The Sb containing shear specimen still consists mainly of large grains; however, the grain boundaries are diffuse rather than distinct.

3.2 Mechanical Properties

TENSILE BEHAVIOR: Stress-strain curves for the tensile tests are shown in Figure 16. Each curve represents a single specimen. The tensile strengths range from 86 MPa for the 58Sn-40Pb-2In to 96 MPa for the 58Sn-40Pb-2Bi.

SEM fractographs of the tensile specimens are shown in Figures 17 and 18. The fracture surfaces of the 60Sn-40Pb, 58Sn-40Pb-2In, and 58Sn-40Pb-2Sb specimens are similar. The Cu_6Sn_5 bulk intermetallics are cleaved while the Sn-Pb matrix appears ductile. The 58Sn-40Pb-2Bi tensile specimen shows an alternate fracture path. The fracture surface of the Bi containing specimen shows an interfacial failure: the crack propagates both through the interfacial Cu_6Sn_5 and between the Cu_6Sn_5 and the solder.

Micrographs of the cross-sections of the fractured tensile specimens are shown in Figures 19 and 20. All alloys reveal Cu_6Sn_5 bulk intermetallics cracking below the fracture surface.

SHEAR BEHAVIOR: Stress-strain curves for the shear tests are shown in Figure 21, each curve representing a single specimen. Shear strengths range from 18 MPa to 26 MPa. Again, the lowest and highest strength values correspond to the 58Sn-40Pb-2In and the 58Sn-40Pb-2Bi alloys, respectively.

The micrographs of the shear fracture profiles are shown in Figures 22 to 25. The fracture profiles of the 60Sn-40Pb and 58Sn-40Pb-2Sb shear specimens show the cracks propagating along eutectic grain boundaries. The 58Sn-40Pb-2In and 58Sn-40Pb-2Bi shear specimens fail near the interface; the crack propagates through the eutectic grains, following no apparent microstructural features.

TENSILE VS. SHEAR: The tensile and shear strengths for all alloys tested are summarized in Figure 26. The relative strengths of the alloys are the same in tension as in shear. The highest to lowest values of strength are obtained for: 58Sn-40Pb-2Bi, 58Sn-40Pb-2Sb, 60Sn-40Pb, and 58Sn-40Pb-2In.

4. DISCUSSION

4.1 Microstructure

60Sn-40Pb: The microstructure observed for the 60Sn-40Pb specimen is typical of a Pb-rich near-eutectic binary alloy. Dendrites of primary α are the first to form on cooling from the melt. As dendrite growth proceeds, solute is rejected into the liquid until the composition of the liquid reaches the eutectic composition, and solidification of the remaining liquid takes place.

EUTECTIC STRUCTURES: Eutectic solidification, the simultaneous solidification of two phases from the liquid phase, is more complex and generally not as well understood as single phase solidification. Single phase structures can be described in terms of individual grains which are building blocks of the aggregate material. This is also true of eutectic structures; however, the single term "grain" does not suffice in describing the relevant features of eutectic structures. Since the terminology used in describing eutectic structures is not conventional, it is worthwhile to define the terms which are used in this study.

The definitions used in this study are in accord with those established by Weart and Mack.[8] Three characteristic features of eutectic structures are:

1) phase particles - the individual particles of the separate phases,
2) eutectic colonies - aggregates of phase particles in which the particles have some characteristic arrangement, and
3) eutectic grains - the portion of the structure that nucleated at a certain site and/or in which the phase particles have definite crystallographic and metallographic relationships to one another.

These three features are illustrated schematically in Figure 27. Although all three features are present in some eutectic structures, colonies need not be present in all eutectic structures.

TERNARY ALLOYS: Comparison of the eutectic microstructure in the In, Bi, and Sb ternaries to the 60Sn-40Pb shows refinement of the eutectic grains and the appearance of diffuse grain boundaries with the addition of the ternary elements. These variations can be explained by considering the effect of the third element on solidification.

The $L \rightarrow \alpha+\beta$ transformation occurs by a nucleation and growth process. The α and β phases solidify by first forming stable nuclei then growing until the grains of $\alpha+\beta$ impinge upon one another. Grain refinement during solidification is possible when the rate of nucleation increases with respect to the rate of growth. This can be accomplished through enhanced nucleation or hindered growth.

Alloying elements may act as nucleation catalysts when the addition results in the formation of intermetallic compounds which then act as heterogeneous nucleation sites. No intermetallic compounds with In, Bi, or Sb are observed in this system, hence, this does not seem likely. Also, an increase in the number of nuclei would not account for the dramatically different appearance of the grain boundaries with alloying.

Both the diffuse grain boundaries and the smaller grain size can be rationalized by a reduction in the growth rate. First consider the role of growth rate in nonequilibrium solidification of a single phase binary alloy, then extend the appropriate analogies to a two-phase ternary system.

The system is modeled by assuming the following experimental conditions:

1) no diffusion in the solid,

2) diffusional mixing in the liquid (i.e., no convection or mechanical stirring).

This condition was considered by Tiller et al.[9] for solidification of a single phase binary alloy. The liquidus and the solidus were approximated as linear functions of composition (Figure 28). This defines a segregation coefficient, k, as:

$$k = C_S/C_L$$

where C_S is the equilibrium concentration of the solid and C_L is the equilibrium concentration of the liquid. For $k<1$, the solid formed is lean in solute with respect to the

liquid; for $k>1$, the solid formed is rich in solute with respect to the liquid. To maintain equilibrium at the solid/liquid interface, solute atoms must be rejected by the solid forming a solute-rich layer in the liquid ($k<1$) or accepted by the solid forming a solute-depleted layer in the liquid ($k>1$), Figure 29. For the remainder of the explanation, consider the case of $k<1$.

Nonequilibrium solidification is most readily explained by considering the two extreme cases of constant temperature and constant growth rate. At a constant temperature, solidification can only proceed at the rate at which solute atoms can diffuse away from the interface. At a constant rate, solidification can only proceed if the temperature of the interface is dropped and the solid increases in solute concentration.

Two-phase solidification of a ternary alloy is analogous to single phase solidification of a binary alloy. In a ternary alloy, the transformation $L \rightarrow \alpha+\beta$ can occur with either temperature or composition as an independent variable. As the α and β solidify, the first material to solidify is lean in the ternary element. The ternary solute species is rejected by the solid, forming a solute rich region in the liquid ahead of the solid/liquid interface.

At a constant temperature, the growth rate continuously decreases since the solute atoms must diffuse away from the interface before solidification can continue. This solidification condition, in which the growth rate continually decreases, would result in a gradual coarsening of the phase particles from the interior of the grain outward.

At a constant growth rate, solidification continues at a continuously decreasing temperature and hence the solid becomes richer in solute. This condition has an indirect effect on the growth rate. Continued solidification requires increased undercooling, which consequently increases the driving force for nucleation. The growth rate decreases with respect to the nucleation rate, resulting in a refined grain size.

The actual solidification condition cannot be described by either of the two extreme cases. Since the quartz crucible was submerged in ice water, the solidification

temperature was not constant, but continuously decreased. On the other hand, constant growth rate requires exact control of the solidification environment which was not expected from the experimental conditions used in this study. Thus, the experimental solidification condition can be described by a combination of the two conditions. Grain refinement with alloying may be explained by both the slower growth rate required for solute diffusion or the enhanced nucleation from increased undercooling. Diffuse grain boundaries may be explained by the continuously decreasing growth rate which results in the formation of a continuously coarser microstructure.

INTERMETALLICS: The formation of intermetallic compounds is a sign of good mutual interdiffusion between the base metal and the solder. The continuous intermetallic layers indicate adequate wetting and solderability. All alloys tested exhibit continuous interfacial intermetallic layers; this is consistent with the fact that none of the alloys posed any difficulty during soldering.

The Cu_6Sn_5 bulk intermetallics have been observed in studies by Frear et al.[10] The intermetallics have been proposed to form at the interface by a screw dislocation mechanism when the molten solder comes in contact with the Cu base metal. After formation, the intermetallic breaks from the surface and the high energy dislocation core dissolves, leaving the intermetallic filled with solder.

TENSILE VS. SHEAR: The variation between the microstructures in the tensile and shear configurations can be attributed to the differences in cooling rates. The tensile specimens cool faster since their fabrication requires less material and a higher ratio of solder to Cu. Thus, the tensile specimens are expected to have a finer microstructure than the shear specimens, as is observed. Also, because the fabrication of the shear specimens requires more material, uniform cooling conditions throughout the specimen are more difficult to maintain. This results in a variation in microstructure along the length of the specimen. This can also lead to density segregation of the Pb-rich α-dendrites in the shear specimens causing a variation in the amount of primary α along the length of the

specimen. Thus, when considering the effect of the ternary addition on microstructure, the microstructures of the tensile specimens should be considered representative.

4.2 Mechanical Properties

TENSILE BEHAVIOR: The joint tensile strengths are high compared to the corresponding bulk tensile data. Manko[1] reports an ultimate tensile strength of 52 MPa for 60Sn-40Pb solder. Since the butt joint specimen tests the solder in a constrained condition it is reasonable that the joint strengths be considerably higher than the bulk strengths.

The failure mode of the tensile specimens is similar for all alloys tested. The Cu_6Sn_5 bulk intermetallics act as preferential initiation sites for cracks. The initiation of the failure at the Cu_6Sn_5 is verified by the cross-sections of the fractured specimens, showing the bulk intermetallics cracking below the fracture surface. The tensile strengths vary for the different alloys. Frear et al.[10] found that the presence of the bulk intermetallics affected the failure mode but not the strength; thus, the differences in strength can be attributed to variations in matrix deformation due to the presence of the ternary element.

The highest joint tensile strength is obtained with the addition of Bi. Although SEM fractography indicates that the specimen fails at the interfacial Cu_6Sn_5, the fracture profile reveals cracking of the bulk Cu_6Sn_5 beneath the fracture surface, similar to the failures of the other alloys tested. This suggests that the strength of the solder slightly exceeds the strength of the interface, most likely a result of the triaxial stress state at the interface from the constraining Cu.

SHEAR BEHAVIOR: Reported shear strengths vary from 19 MPa[11] to 39 MPa[1] for 60Sn-40Pb solder. The lower shear strength was obtained at a crosshead speed of 0.05 mm/min (no corresponding strain rate specified) while the higher value was obtained at a 0.5 min^{-1} strain rate. The value of 21 MPa obtained in this study for 60Sn-40Pb

solder is in line with the range of reported values. Direct comparison of values cannot be made since different specimen configurations[11] and strain rates are expected to yield different results. Furthermore, the reported values are not accompanied by documentation of microstructure tested.

The 60Sn-40Pb and 58Sn-40Pb-2Sb alloys fail in shear at the grain boundaries. In the binary alloy the grain boundaries are distinct while in the Sb containing alloy the grain boundaries are diffuse.

The additions of In and Bi shift the fracture path in shear from the eutectic grain boundaries to the solder near the solder/Cu interface. The microstructural effects of the ternary additions suggest that the change in the crack path is caused by either grain boundary strengthening from the suspect segregation of solute atoms or a reduction in stress concentration at the grain boundaries due to the elimination of distinct grain boundaries. The micrographs of the fracture profiles of the shear specimens show deformation appearing uniform throughout the joints for the In- and Bi-containing ternary alloys, Figures 23(a) and 24(a); this uniform deformation is not apparent in the 60Sn-40Pb specimen. This supports the latter assumption that the formation of diffuse grain boundaries by the addition of ternary elements relieves the stress concentrations at the grain boundaries. However, this does not explain the differences in strength between the In-containing alloy, which yields the lowest strength, and the Bi-containing alloy, which yields the highest strength, and suggests that the ternary additions also account for a change in the inherent strength of the solder.

The presence of the diffuse grain boundaries alone does not alone insure the uniform deformation observed in the In and Bi alloyed shear specimens. The diffuse grain boundaries are also present in the Sb alloyed shear specimen, however, the failure in the Sb alloyed specimen occurs at the grain boundaries. This suggests that the failure path in shear is determined by the heterogeneities in the overall microstructure. Since the grains of the 58Sn-40Pb-2Sb shear specimen are large and the phase particle size within

these grains is fine, the diffuse grain boundaries are heterogeneities. The coarse particle size in the grain boundaries disturbs the overall homogeneity of the joint.

Thus, the failure in shear occurs at heterogeneities for all alloys studied. In the binary 60Sn-40Pb, eutectic grain boundaries act as heterogeneities at which the shear stress concentrates. In the 58Sn-40Pb-2Sb alloy, the coarse-particled, diffuse grain boundaries act as the heterogeneity. In the 58Sn-40Pb-2In and 58Sn-40Pb-2Bi alloys, the microstructure of the solder is homogeneous with diffuse grain boundaries; the solder/Cu interface acts as the heterogeneity at which failure occurs.

TENSILE VS. SHEAR: Although a comparison of the constitutive behavior of the tensile and shear mechanical data seems appropriate, speculation of the strengths shows that the conversion of the data to equivalent stress-strain curves by assuming simple tension and simple shear loading conditions would not be applicable. The tensile strengths obtained are approximately 4 times higher than the shear strengths, rather than the theoretical value of 1.7. This comparison is not possible since the high constraint of the tensile specimen configuration results in a triaxial stress state, making the simple tension approximation inappropriate. However, it should be noted that the relative strengths of the alloys are consistent between the tensile and shear tests in this study.

4.3 Alloy Development

Although the information presented in this study cannot be used directly to infer a more fatigue resistant solder alloy, candidate alloys may be suggested for further study.

Studies of joints of binary eutectic and near-eutectic solders in thermal fatigue have shown that upon cycling, a heterogeneous coarsening -- a coarsening of the phase particle size in a localized region of the joint -- occurs.[12-16] This coarsening continues until a crack initiates and propagates through the coarsened region. Although this coarsening is not well understood, a proposed mechanism states that the coarsening begins at heterogeneities in the joint.[12] If this deformation is similar to the slow strain

rate deformation in shear performed in this study, it is possible that the heterogeneities of the distinct eutectic grain boundaries are the cause of the initial coarsening. Hence, a desirable microstructure would be one in which the overall microstructure is homogeneous. Since the additions of In and Bi result in a homogeneous microstructure which contains diffuse grain boundaries and the deformation of such joints in shear exhibits uniform deformation throughout the joints, these elements are attractive candidates for further study.

Regardless of the mechanism involved in the coarsening during thermal fatigue, the properties of the alloys investigated are adequate to warrant further study. The strengths of the ternary alloys are in the range of the binary 60Sn-40Pb solder. Although the addition of In results in lower strengths in both tensile and shear deformation, the strengths are only slightly lower and still adequate for that necessary in packaging applications.[2]

5. CONCLUSIONS

The following conclusions were obtained from this study of the effects of ternary additions of In, Bi, and Sb on the microstructure and tensile and shear behavior of near-eutectic Sn-Pb base alloys:

1. The 60Sn-40Pb microstructure consists of primary α-dendrites in a eutectic matrix of α-Pb and β-Sn. The matrix is composed of eutectic grains with distinct grain boundaries.

   Ternary additions of In, Bi, and Sb alter the microstructure by refining the eutectic grain size and introducing diffuse grain boundaries.

2. Tensile failure initiates at Cu_6Sn_5 bulk intermetallics for all alloys tested. The addition of Bi results in the highest increase in strength.

3. Shear failure occurs at heterogeneities in the joint. In 60Sn-40Pb, the failure occurs at the distinct eutectic grain boundaries; in 58Sn-40Pb-2Sb, the failure occurs at the diffuse eutectic grain boundaries. The 58Sn-40Pb-2In and 58Sn-40Pb-2Bi alloys have homogeneous microstructures throughout the joint; shear failure occurs near the interface.

6. REFERENCES

1. H.H. Manko, *Solders and Soldering,* McGraw-Hill, New York, 1979.

2. P.M. Hall, "Solder Attachment of Leadless Ceramic Chip Carriers," *Solid State Technol.,* March 1963, p 103.

3. J.W. Balde, D. Brown, "Alternatives in VLSI Packaging," *VLSI Design,* December 1983, p 23.

4. J. Lyman, "Surface Mounting Alters the PC-Board Scene,"*Electronics,* February 1984, p 113.

5. R.E. Settle Jr., "A New Family of Microelectronic Packages for Avionics," *Solid State Technol.,* June 1978, p 54.

6. C.J. Thwaites, "Soldering Technology -- A Decade of Progress," *Inter. Met. Rev.,* **29** (2), p 45 (1984).

7. D. Frear, D. Grivas, L. Quan, and J.W. Morris Jr., "Microstructural Observations and Mechanical Behavior of Pb-Sn Solder on Copper Plates," *Mat. Res. Symp. Proc.,* **72**, p 181 (1986).

8. H.W. Weart and D.J. Mack, "Eutectic Solidification Structures," *Trans. Met. Soc. AIME,* **212**, p 664 (1958) .

9. W.A. Tiller, K.A. Jackson, J.W. Rutter, and B. Chalmers, "The Redistribution of Solute Atoms during the Solidification of Metals," *Acta Met.,* **1**, p 428 (1953).

10. D. Frear, D. Grivas, J.W. Morris Jr., "The Effect of Cu_6Sn_5 Whisker Precipitates in Bulk 60Sn-40Pb Solder," *J. Electron. Mater.,* **16** (3), p 181 (1987).

11. *Welding, Brazing, and Soldering,* Metals Handbook, American Society for Metals, Metals Park, Ohio, 1983, Vol. 6, p 1092.

12. C.J. Thwaites, "Mechanical Strength of Selected Soldered Joints and Bulk Solder Alloys," *Weld. J.,* **55** (10), p 323s (1976).

13. D. Frear, "Microstructural Observations of the Sn-Pb Solder/Cu System and Thermal Fatigue of the Solder Joint," Ph.D. Thesis, University of California at Berkeley, 1987.

14. R. Yenawine, M. Wolverton, A. Burkett, B. Waller, B. Russel, D. Spitz, "Today and Tomorrow in Soldering," *11th Annual Electronics Manufacturing Seminar Proceedings,* China Lake, CA, p 377 (1987).

15. T.A. Krinke and D.K. Pai, "Solder Joint Failure in Leadless Ceramic Chip Carriers," *12th Annual Electronics Manufacturing Seminar Proceedings,* China Lake, CA, p 241 (1988).

16. W.M. Wolverton, "The Mechanisms and Kinetics of Solder Joint Degradation," *Brazing Soldering,* (13), p 331 (1987).

17. *Metallography, Structures and Phase Diagrams,* Metals Handbook, American Society for Metals, Metals Park, Ohio, 1973, Vol. 8, p 330.

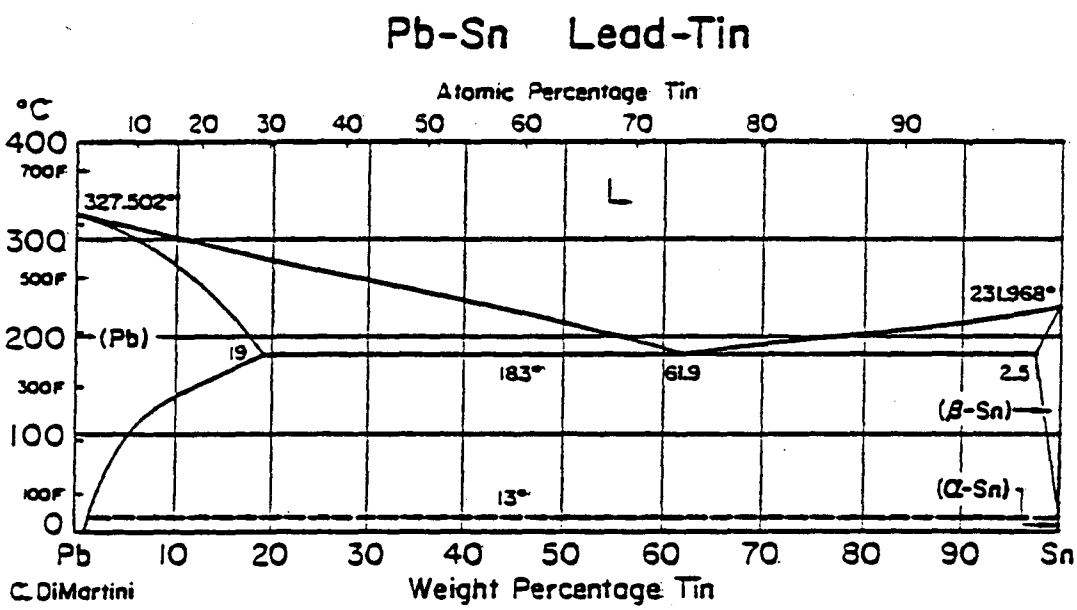

Figure 1: Pb-Sn phase diagram.[17]

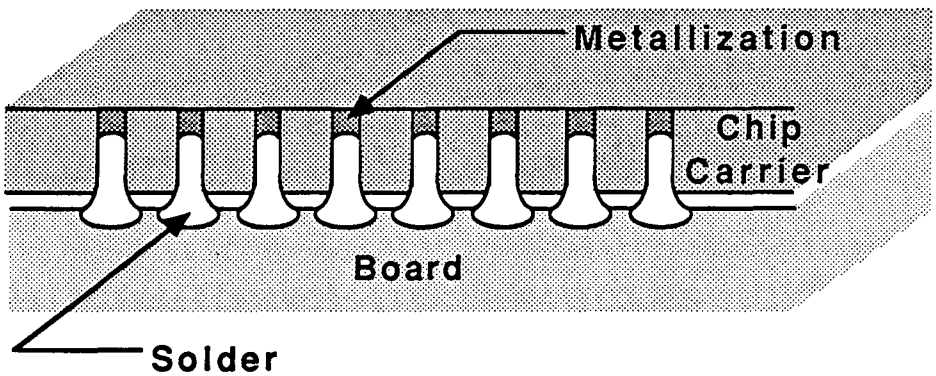

Figure 2: Schematic representation of a surface mounted leadless chip carrier. The solder joins the metallization on the package to a pad on the board.

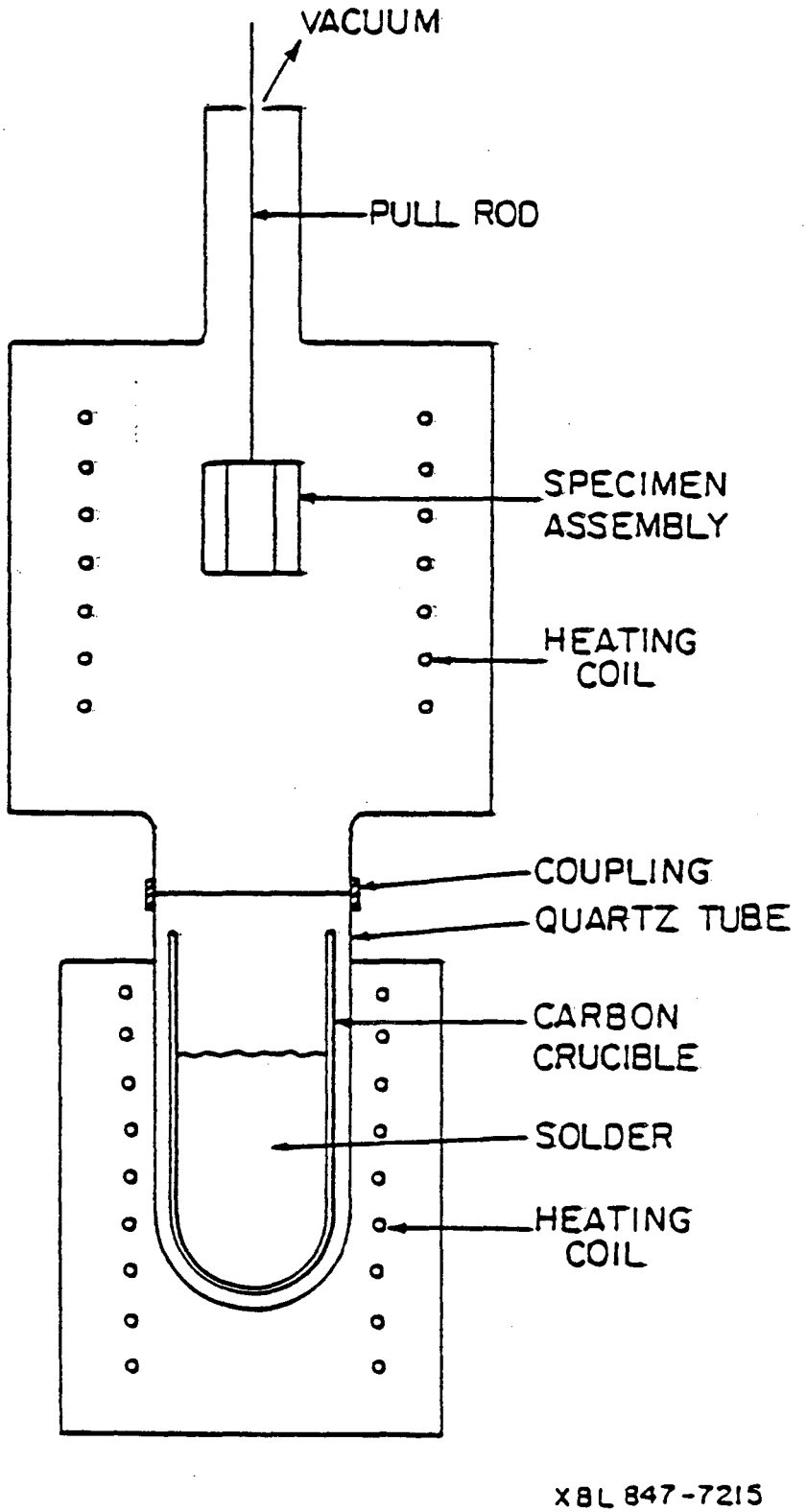

Figure 3: Vacuum furnace configuration used in specimen preparation.

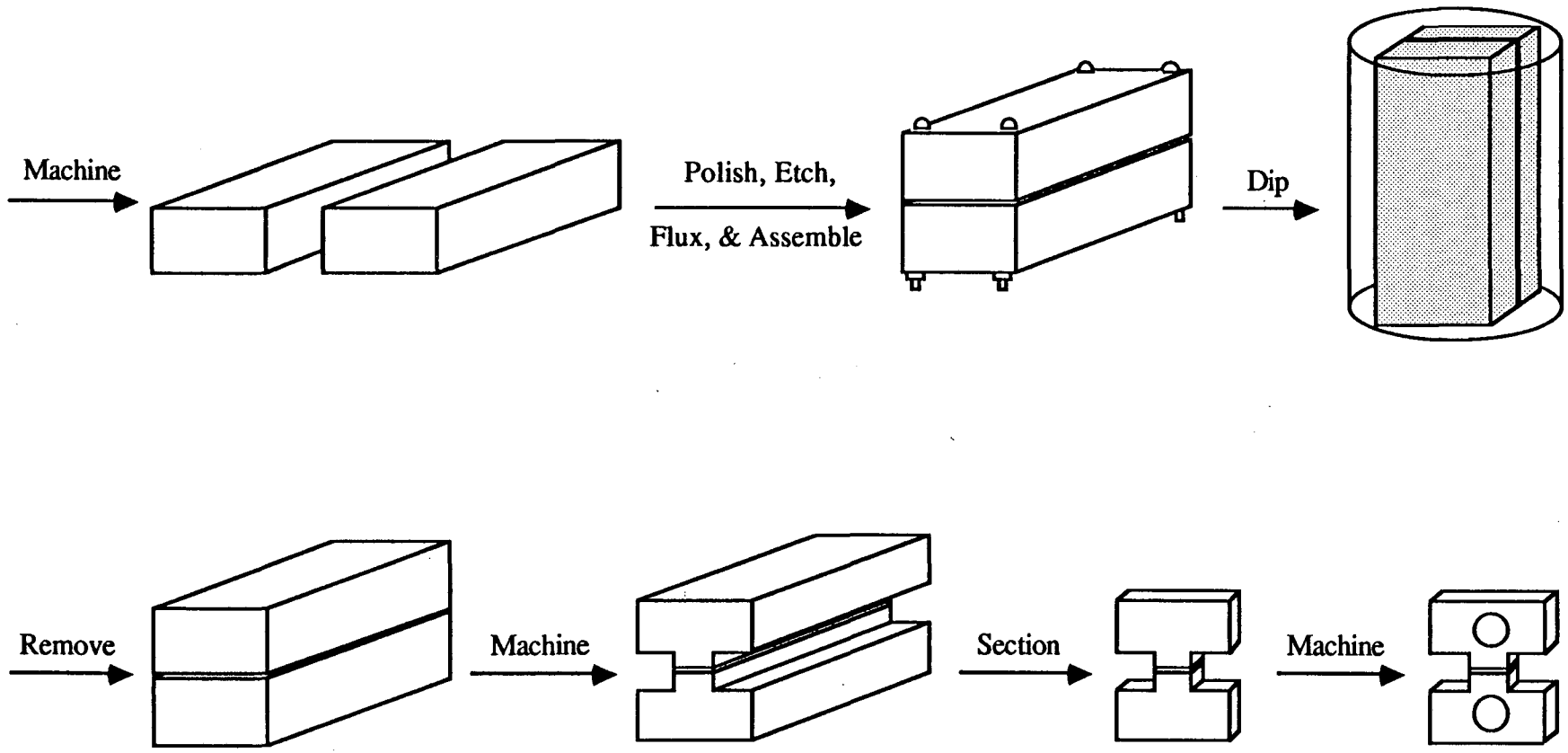

Figure 4: Schematic representation of the tensile specimen preparation process.

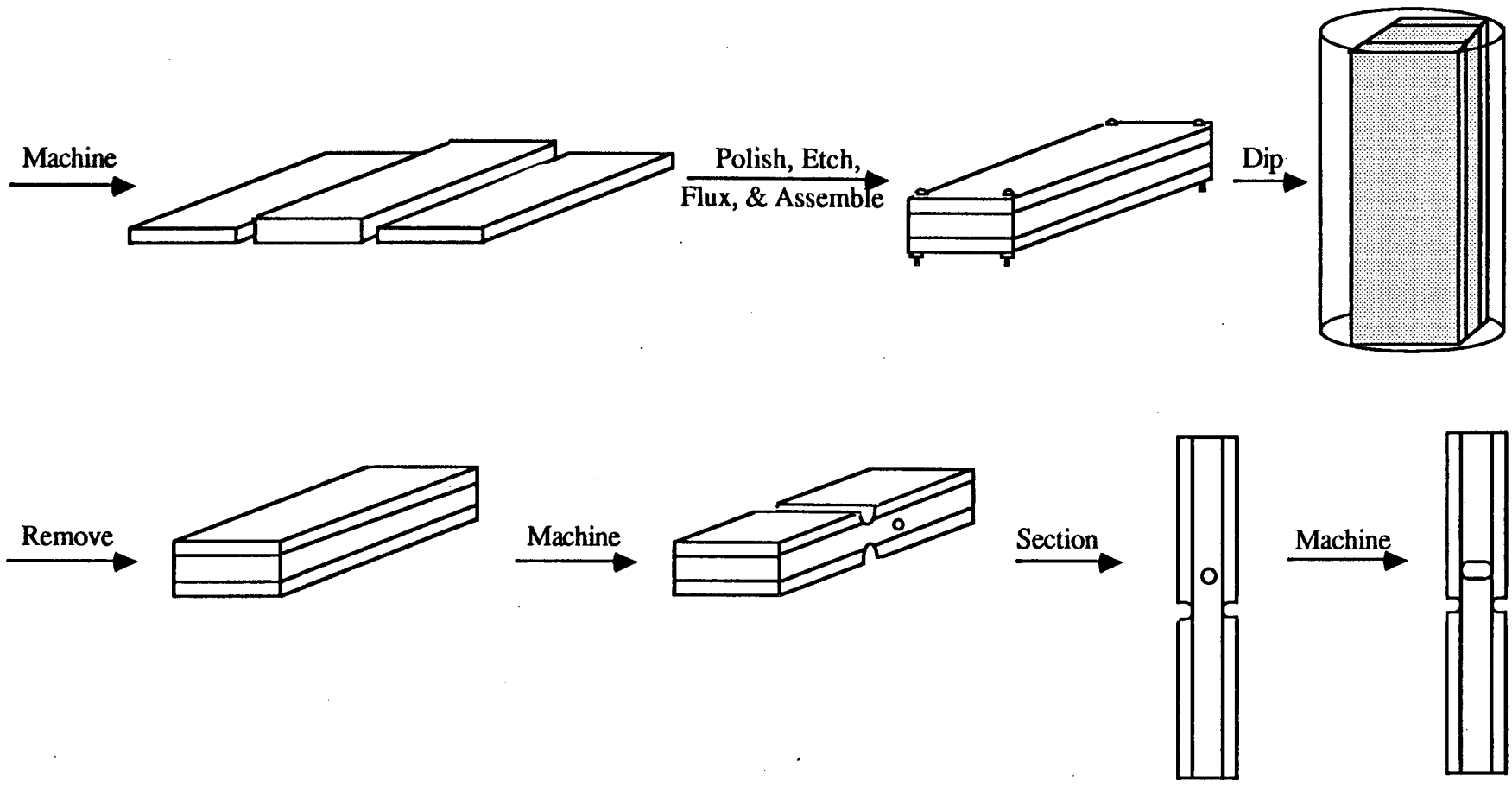

Figure 5: Schematic representation of the shear specimen preparation process.

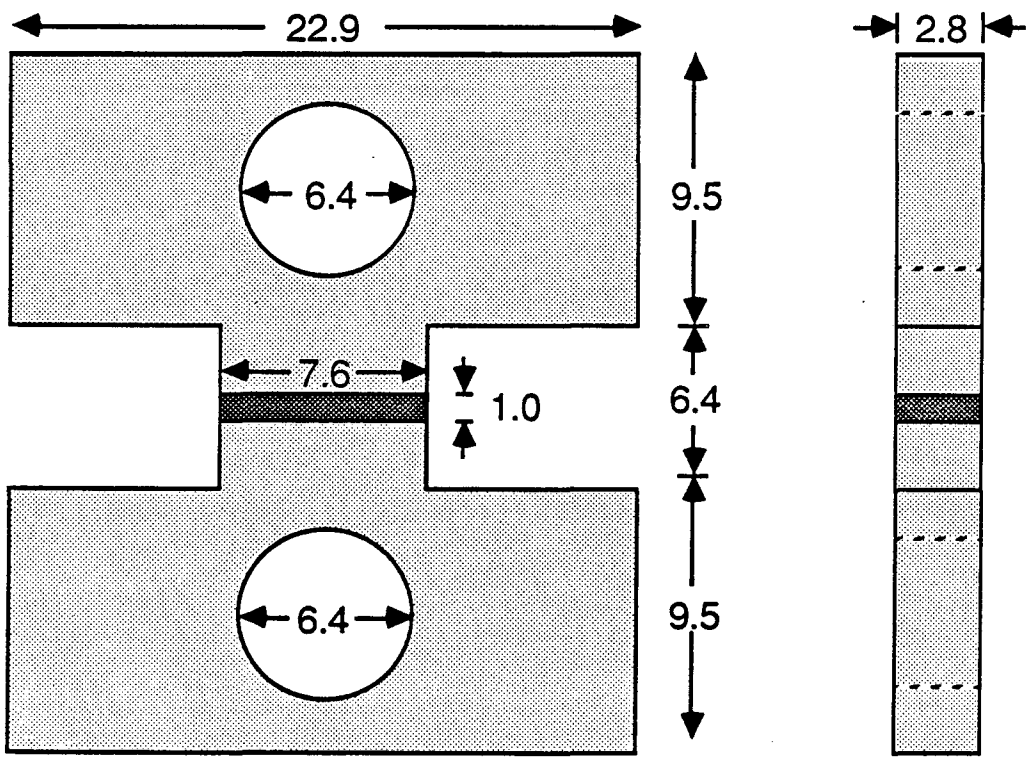

Figure 6: Tensile specimen configuration (dimensions in mm).

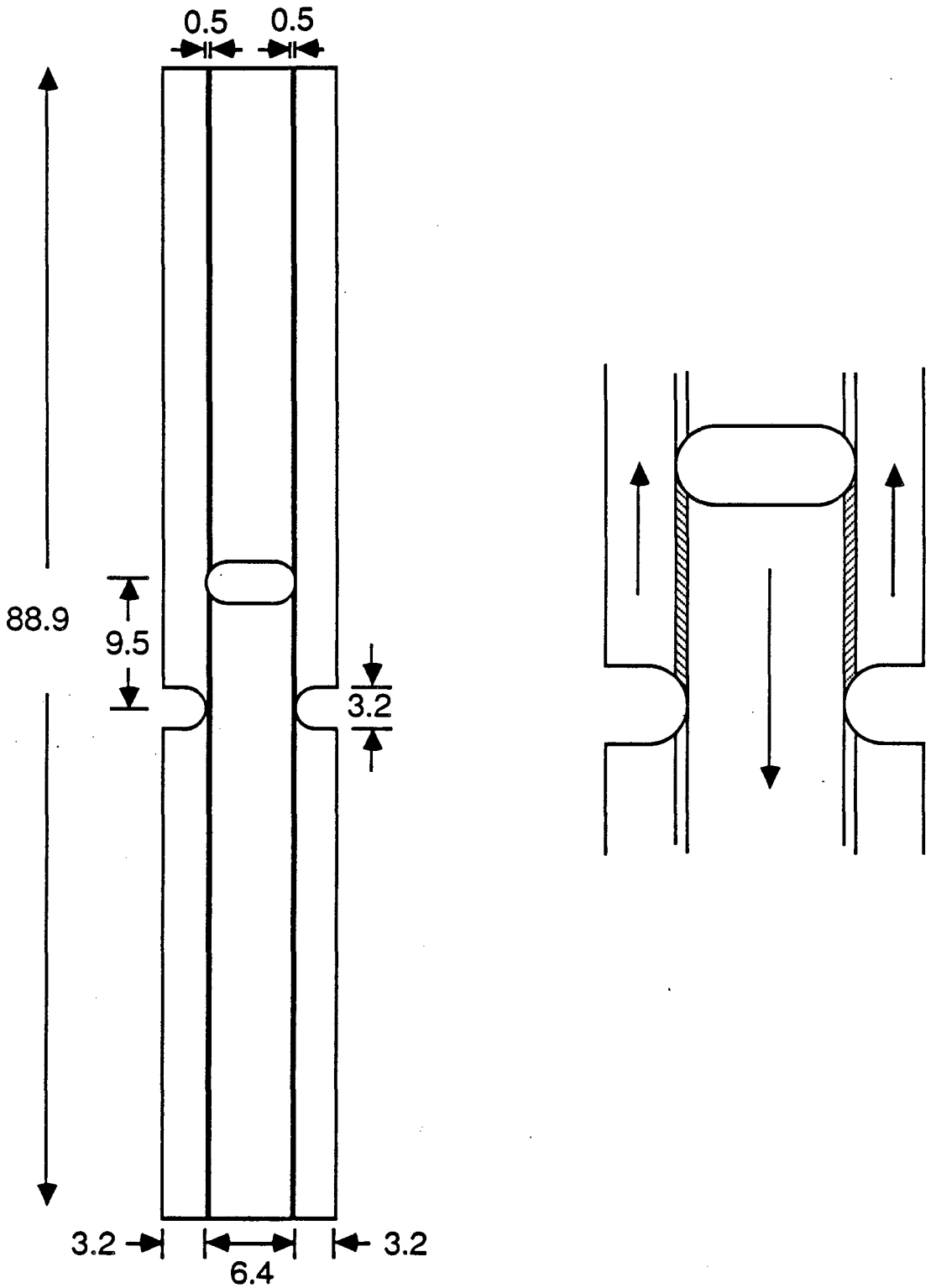

Figure 7: Shear specimen configuration (dimensions in mm).

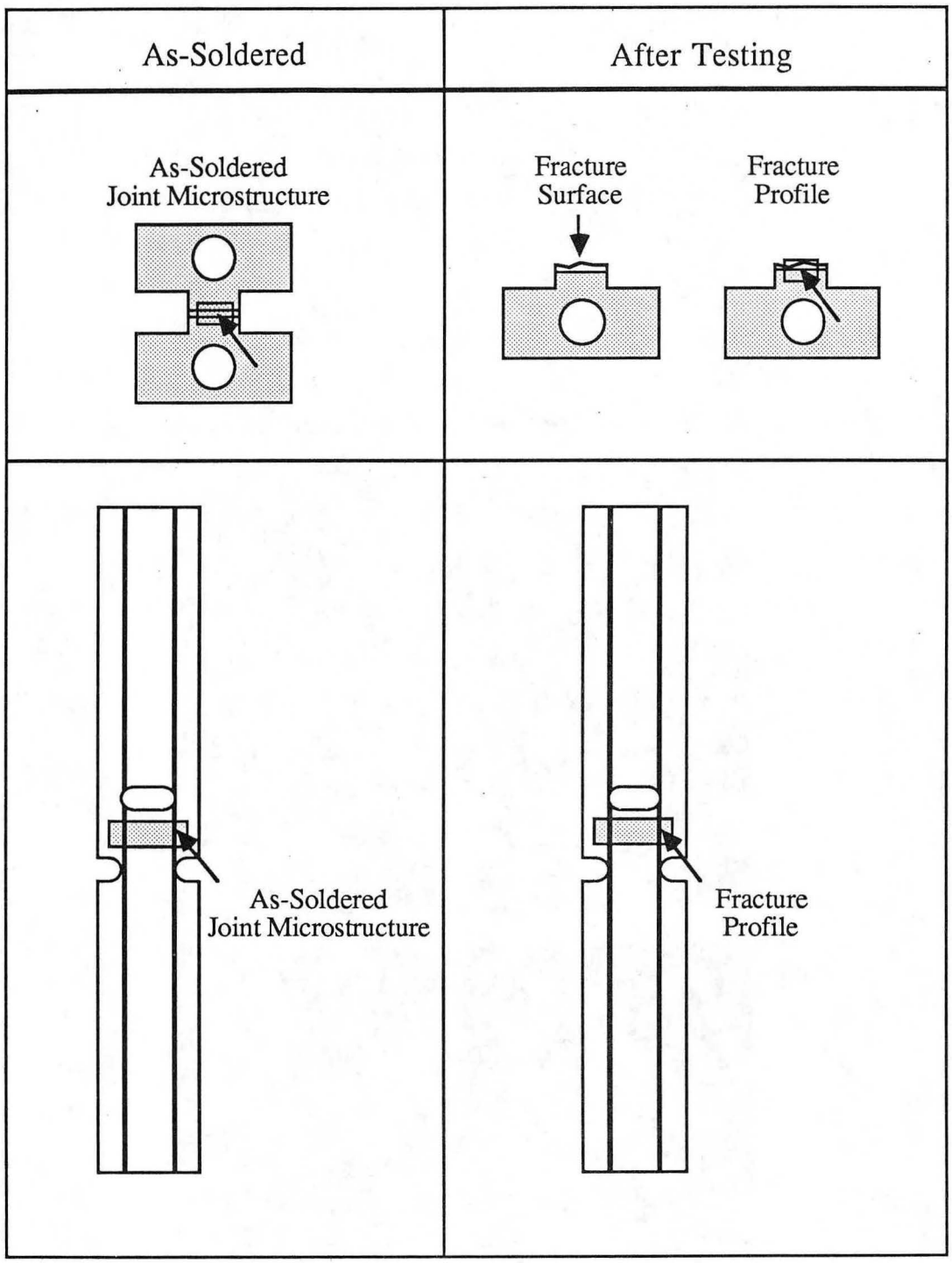

Figure 8: Schematic representation of the joint orientations examined.

(a)

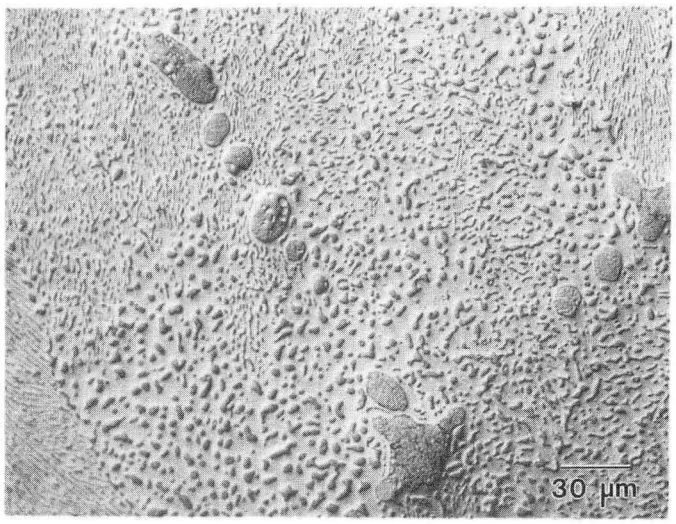

(b)

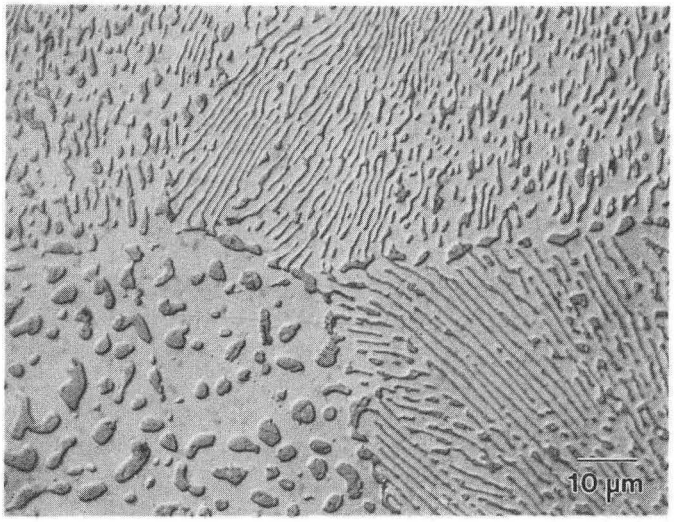

(c)

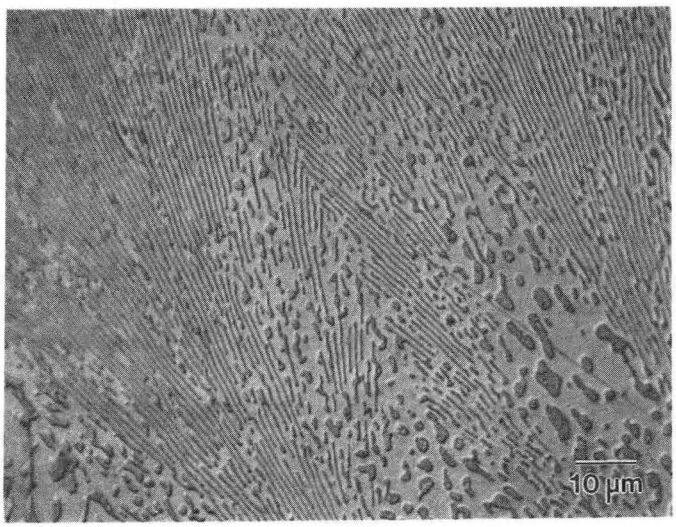

XBB885-5414

Figure 9: Optical micrographs of the 60Sn-40Pb tensile specimen showing: (a) Pb-rich α-dendrites in a eutectic matrix, (b) the variation of morphology from grain to grain and the distinct grain boundaries, and (c) the colony structure within a lamellar grain.

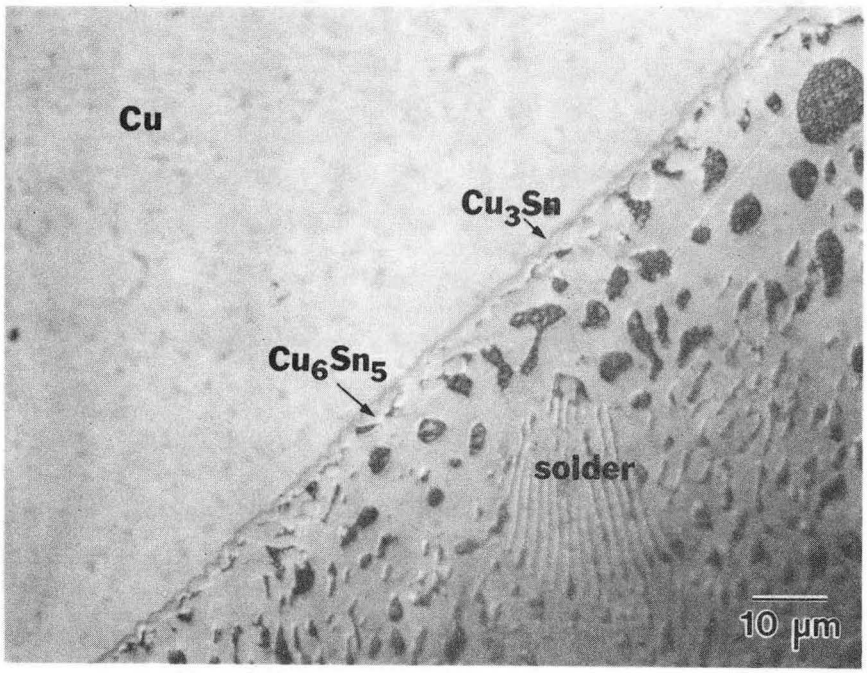

XBB 885-5415

Figure 10: Optical micrograph of the interfacial intermetallics. The Cu_3Sn is adjacent to the Cu and the Cu_6Sn_5 is adjacent to the solder.

(a)

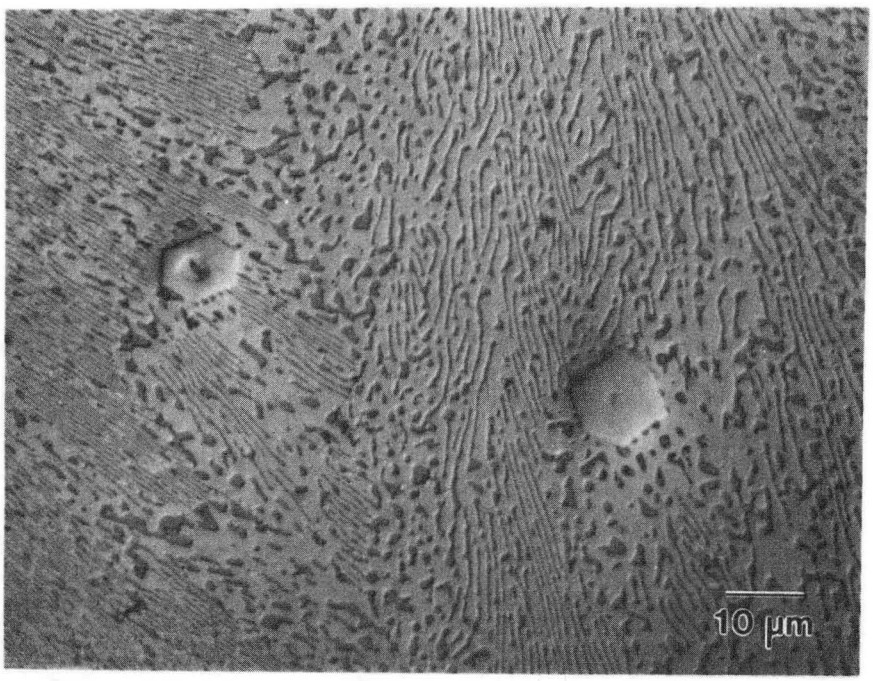

(b)

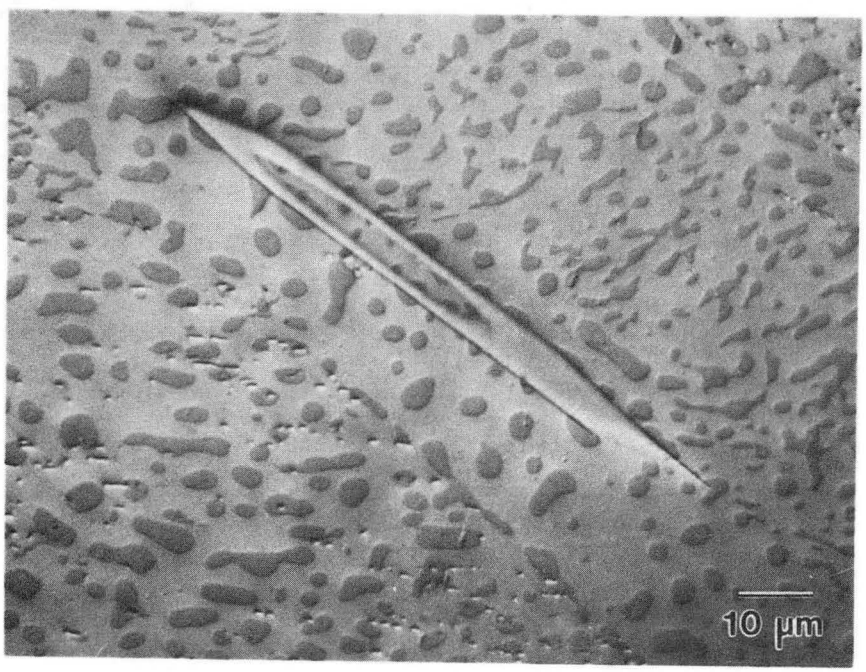

XBB885-5416

Figure 11: Optical micrographs of the bulk Cu_6Sn_5 intermetallic rods. Figure 11(a) is a cross-section showing the hexagonal core; figure 11(b) shows the transverse section of a rod.

(a)

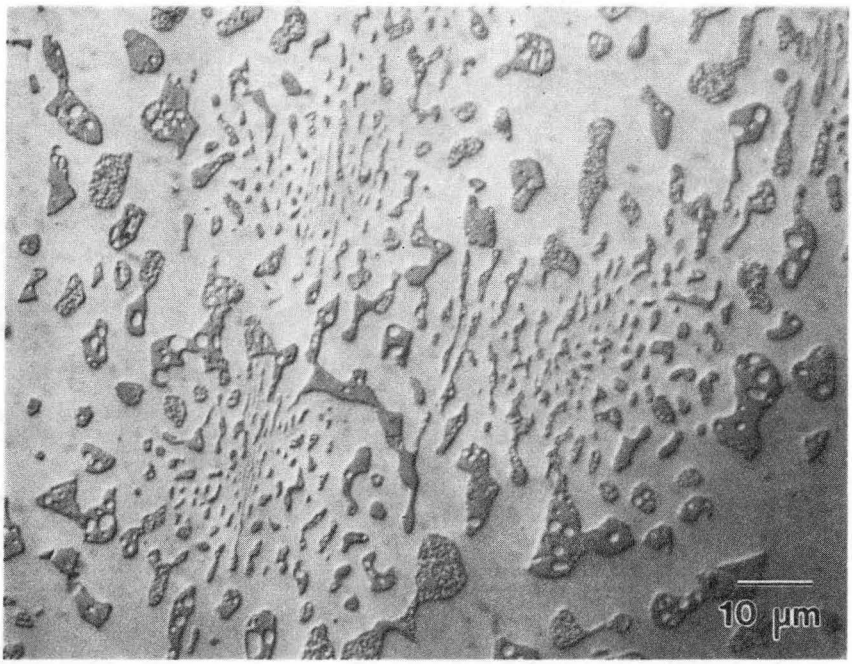

(b)

XBB 885-5417

Figure 12: Optical micrographs of the eutectic structure of (a) the 58Sn-40Pb-2In tensile specimen and (b) the 58Sn-40Pb-2Bi tensile specimen.

(a)

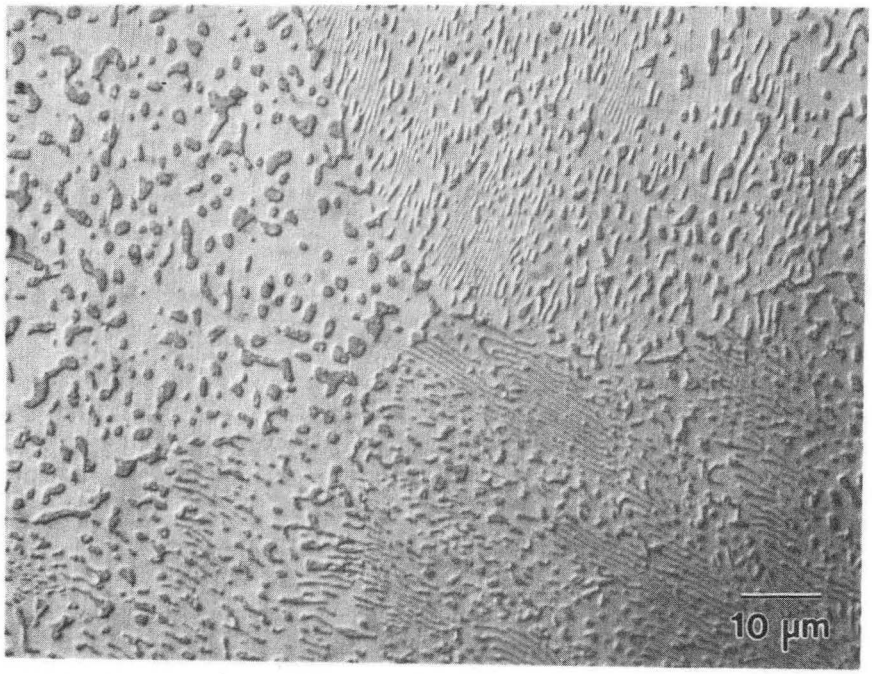

(b)

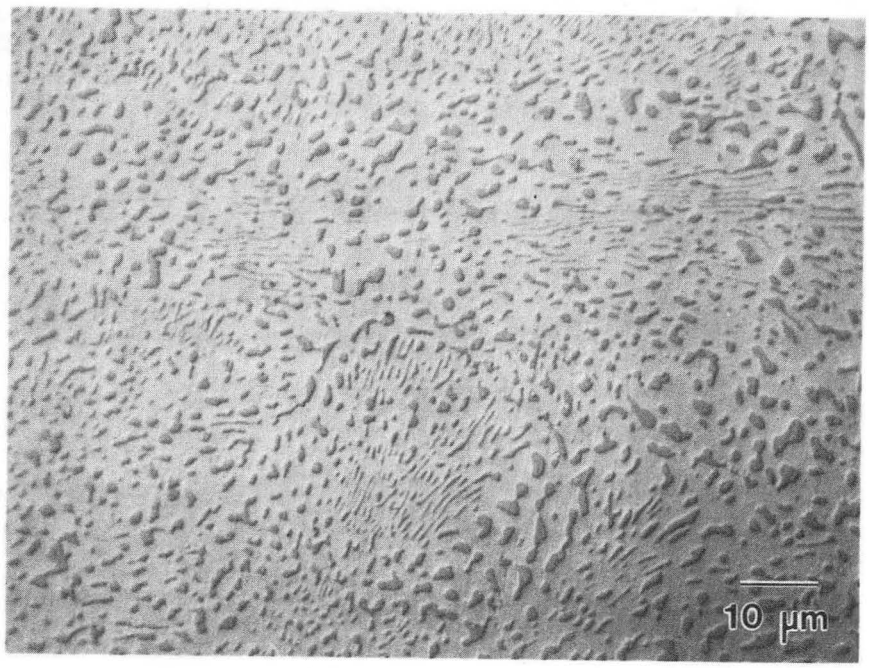

XBB 885-5418

Figure 13: Optical micrographs of the eutectic structure of the 58Sn-40Pb-2Sb tensile specimen. The eutectic grain boundaries are distinct in (a) and diffuse in (b).

(a)

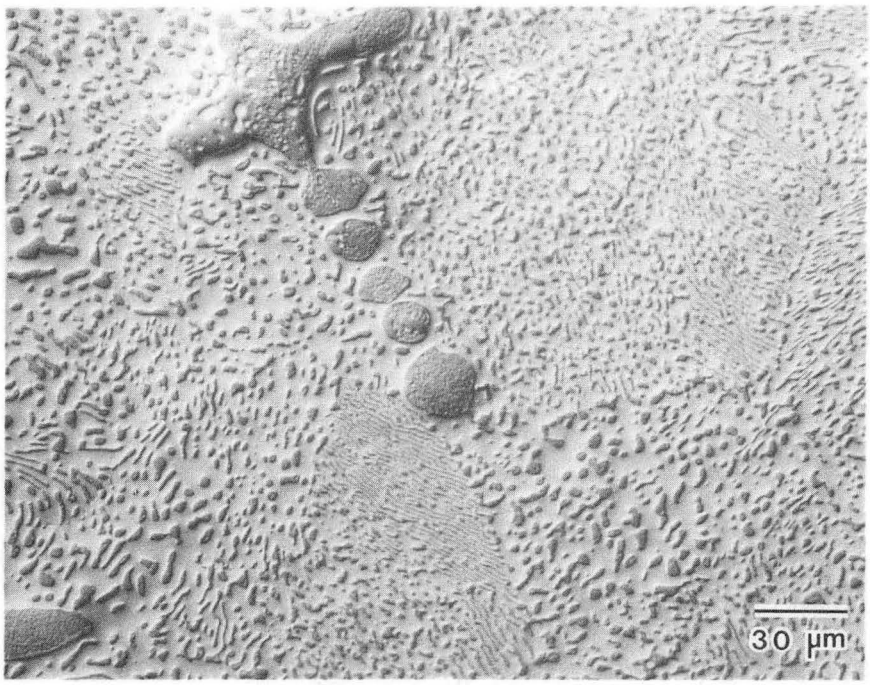

(b)

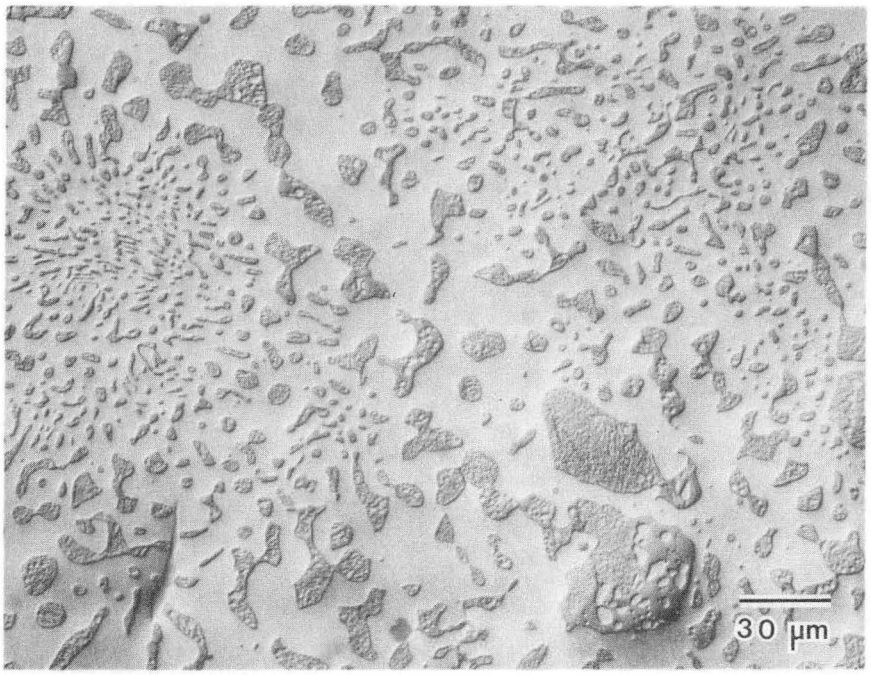

XBB 885-5419

Figure 14: Optical micrographs of (a) the 60Sn-40Pb shear specimen and (b) the 58Sn-40Pb-2In shear specimen.

(a)

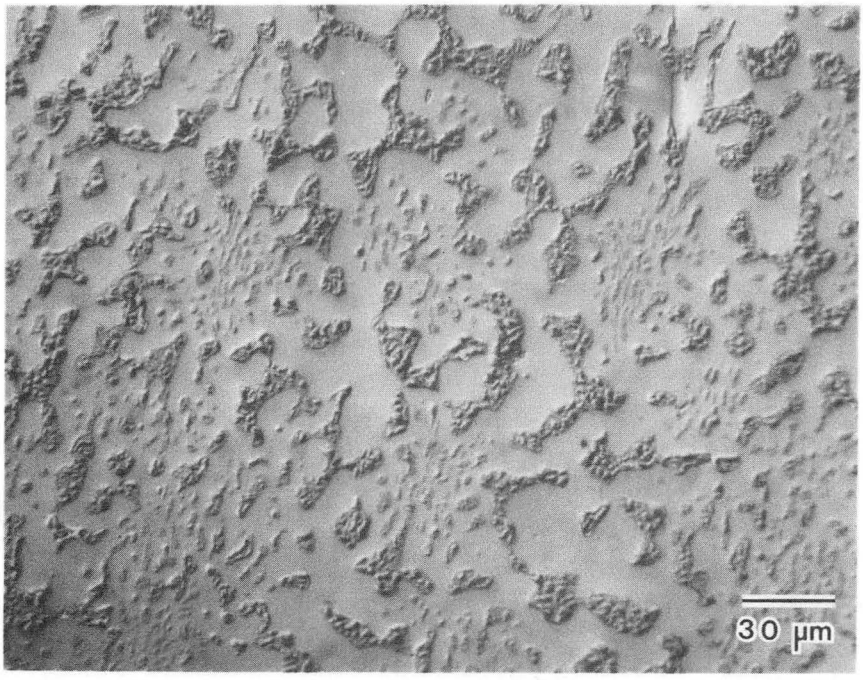

(b)

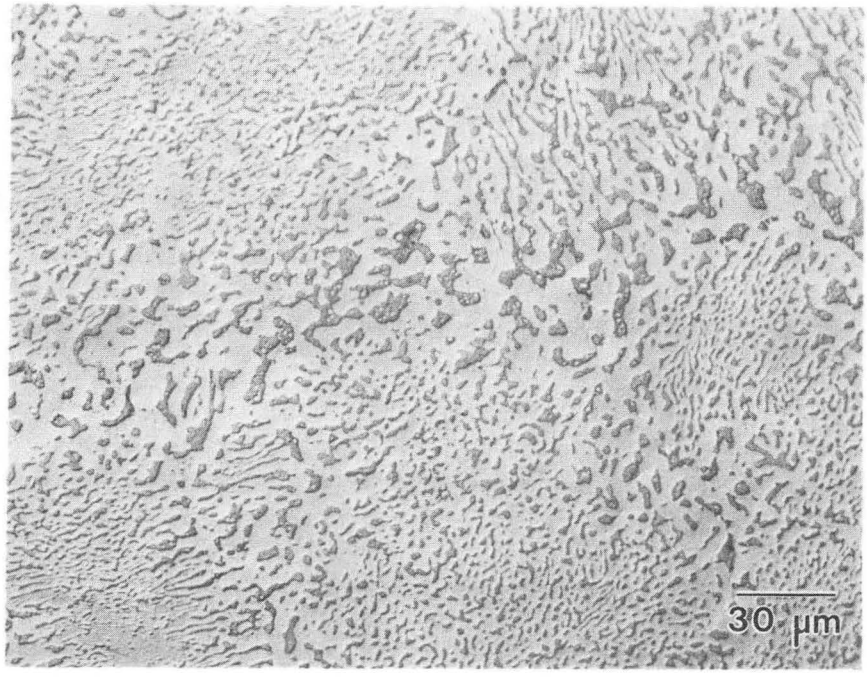

XBB 885-5420

Figure 15: Optical micrographs of (a) the 58Sn-40Pb-2Bi shear specimen and (b) the 58Sn-40Pb-2Sb shear specimen.

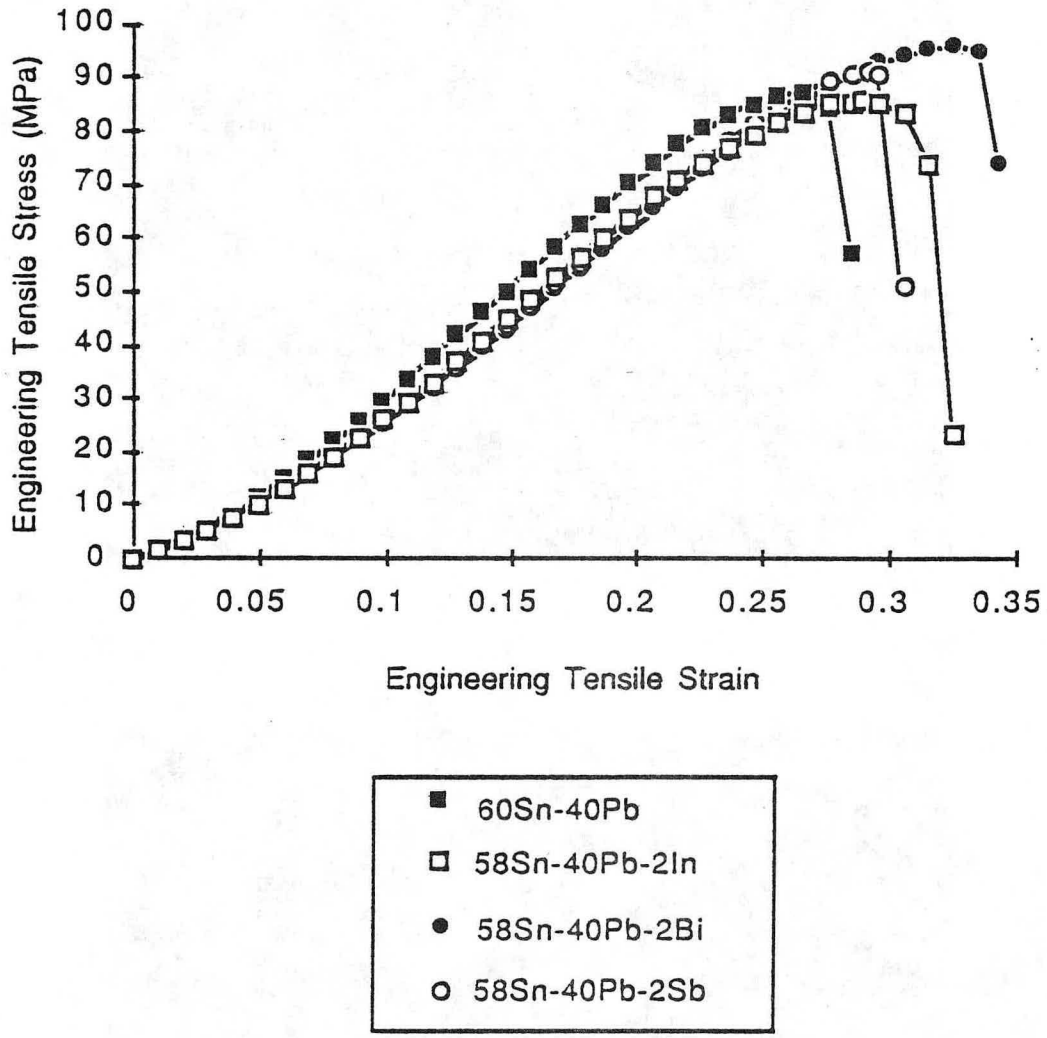

Figure 16: Engineering stress-strain curves for the tensile tests.

(a)

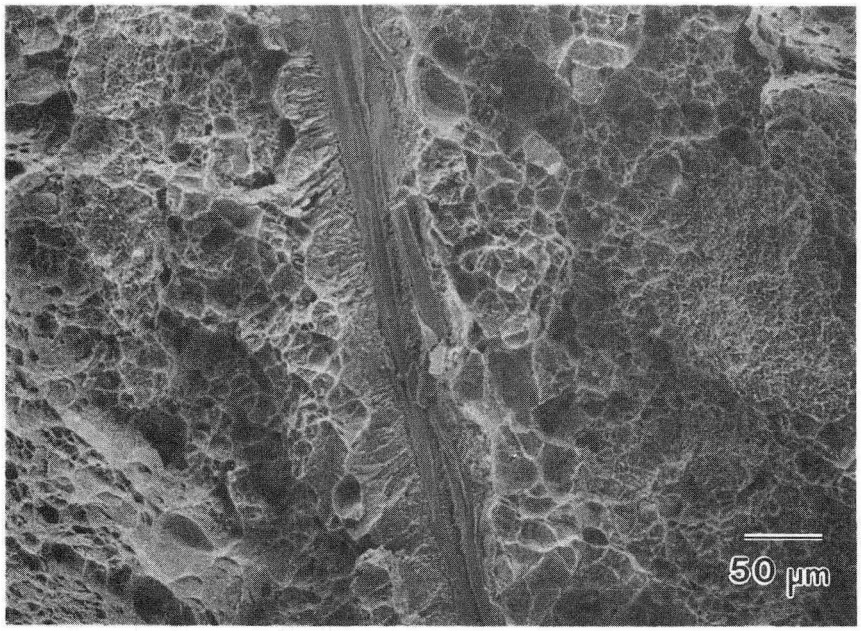

(b)

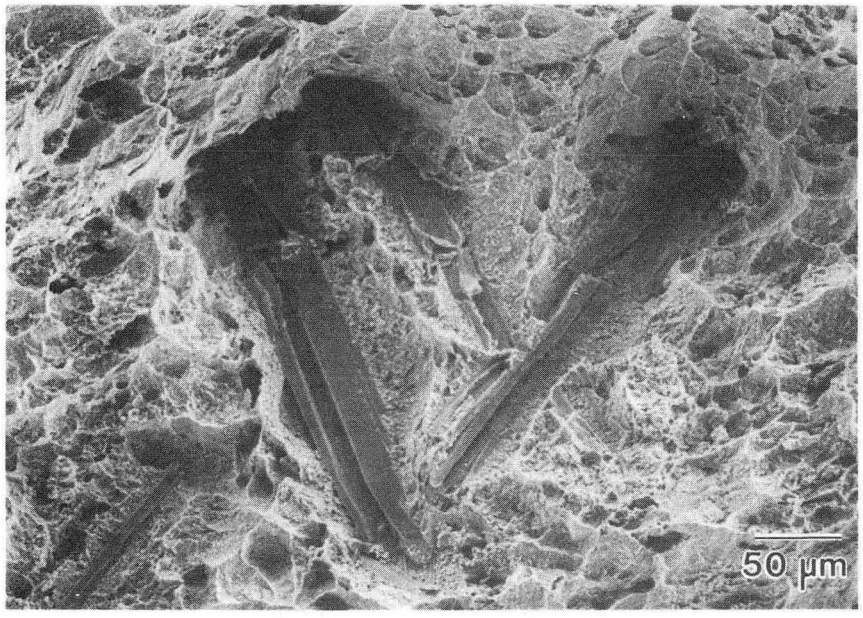

XBB 885-5421

Figure 17: SEM fractographs of (a) the 60Sn-40Pb tensile specimen and (b) the 58Sn-40Pb-2In tensile specimen.

(a)

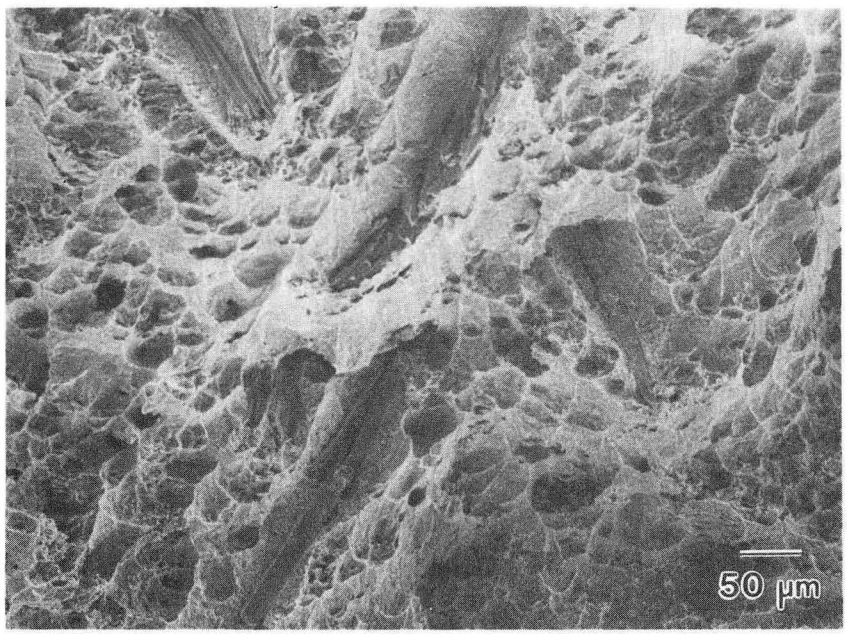

(b)

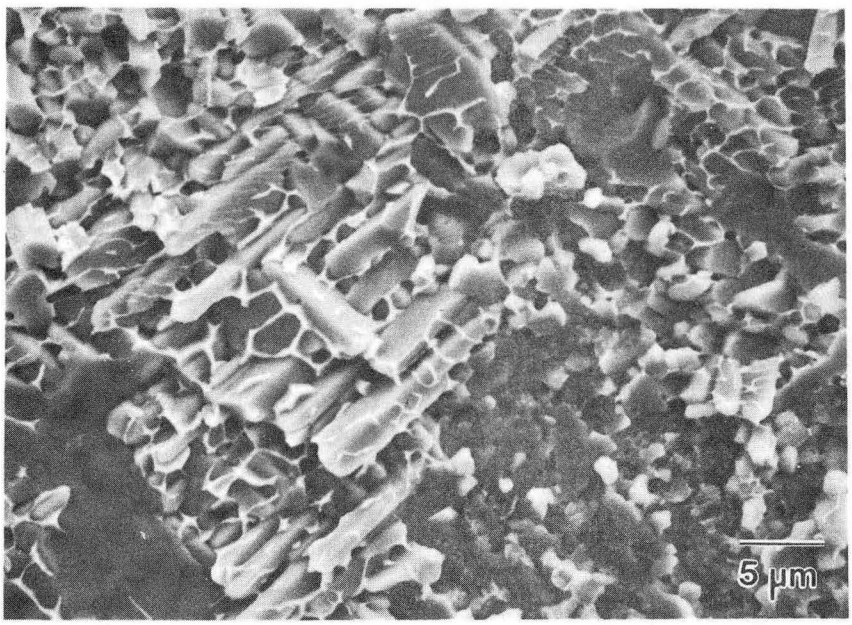

XBB 885-5422

Figure 18: SEM fractographs of the 58Sn-40Pb-2Sb tensile specimen and (b) the 58Sn-40Pb-2Bi tensile specimen.

(a)

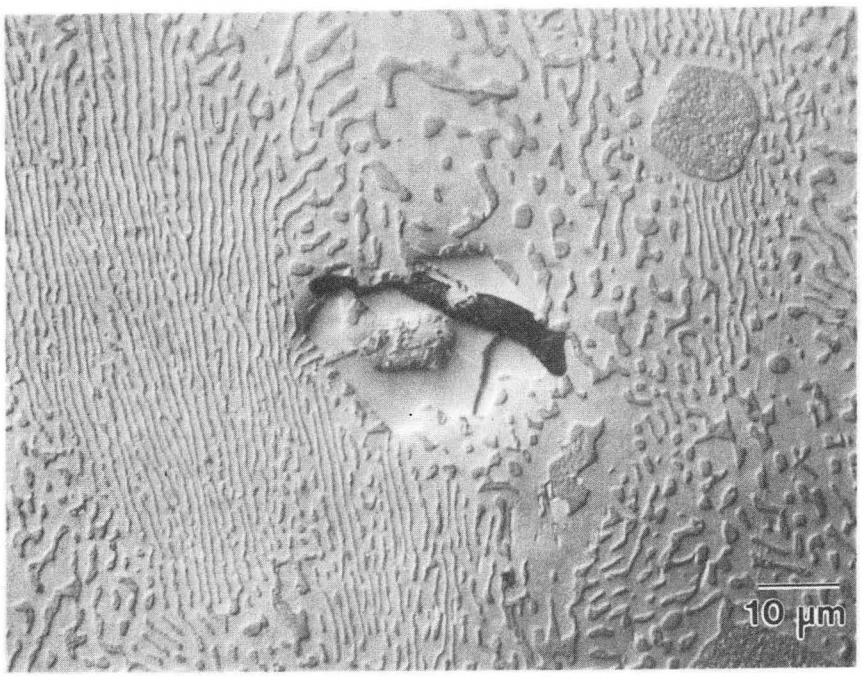

(b)

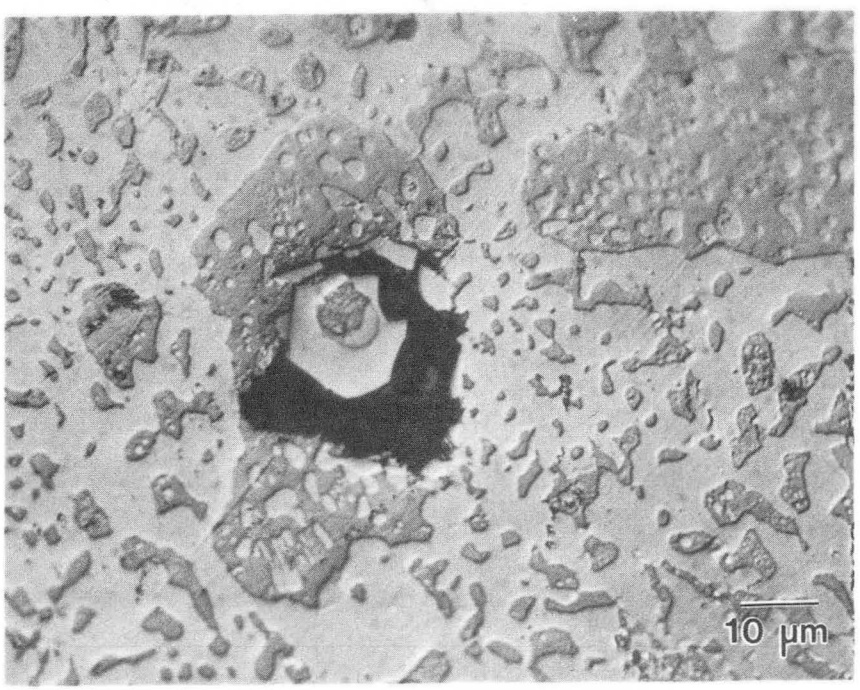

XBB 885-5423

Figure 19: Optical micrographs of the cross-sections below the fracture surface of (a) the 60Sn-40Pb tensile specimen and (b) the 58Sn-40Pb-2In tensile specimen.

(a)

(b)

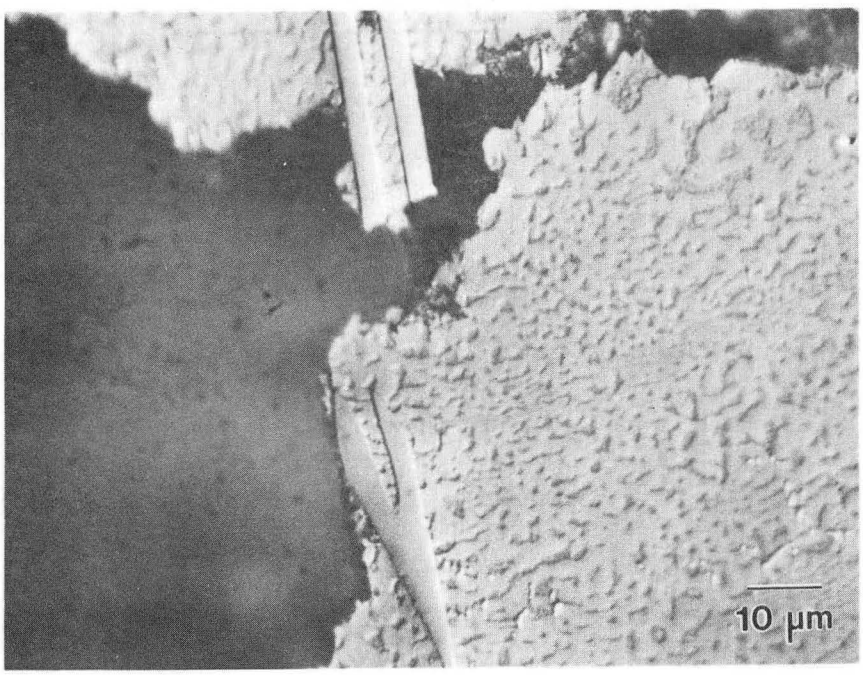

XBB 885-5424

Figure 20: Optical micrographs of the cross-sections below the fracture surface of (a) the 58Sn-40Pb-2Sb tensile specimen and (b) the 58Sn-40Pb-2Bi tensile specimen.

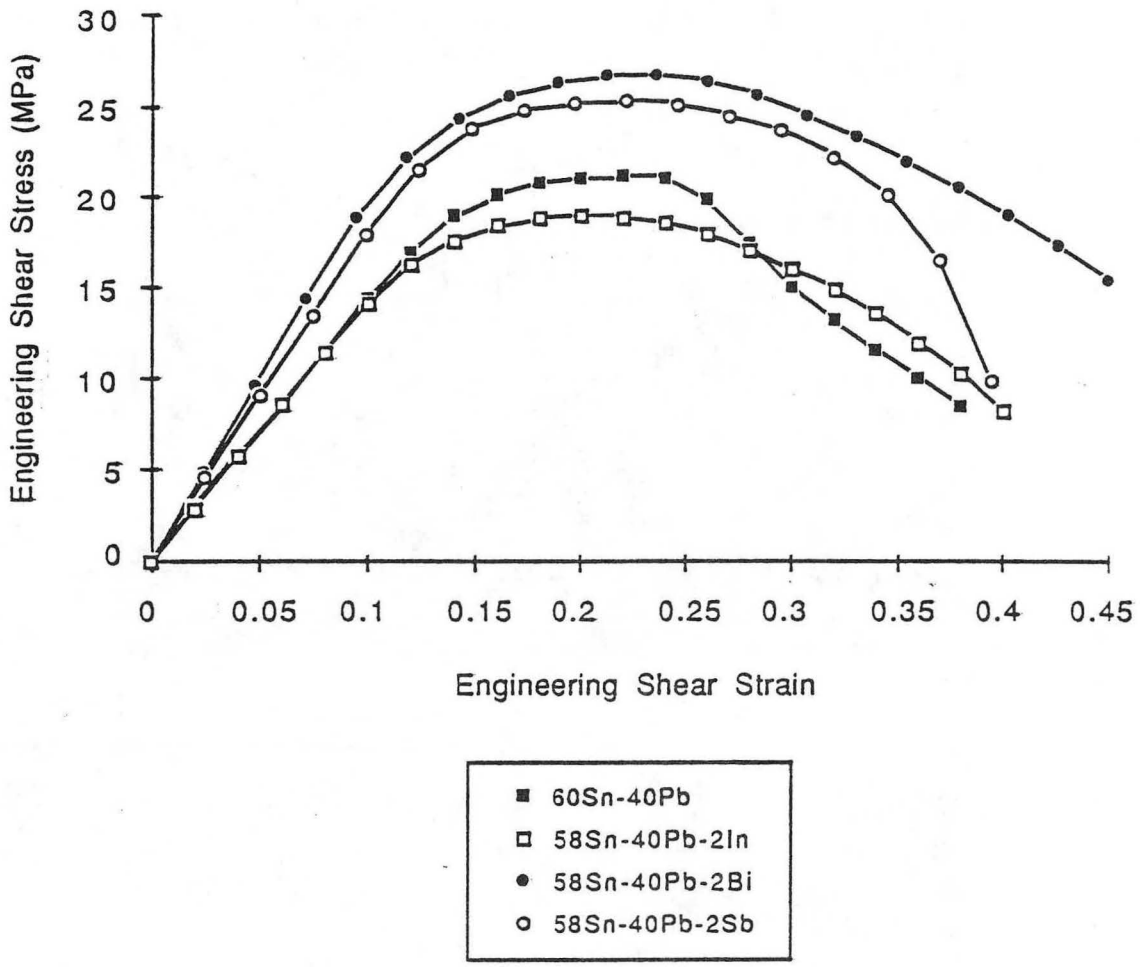

Figure 21: Engineering stress-strain curves for the shear tests.

(a)

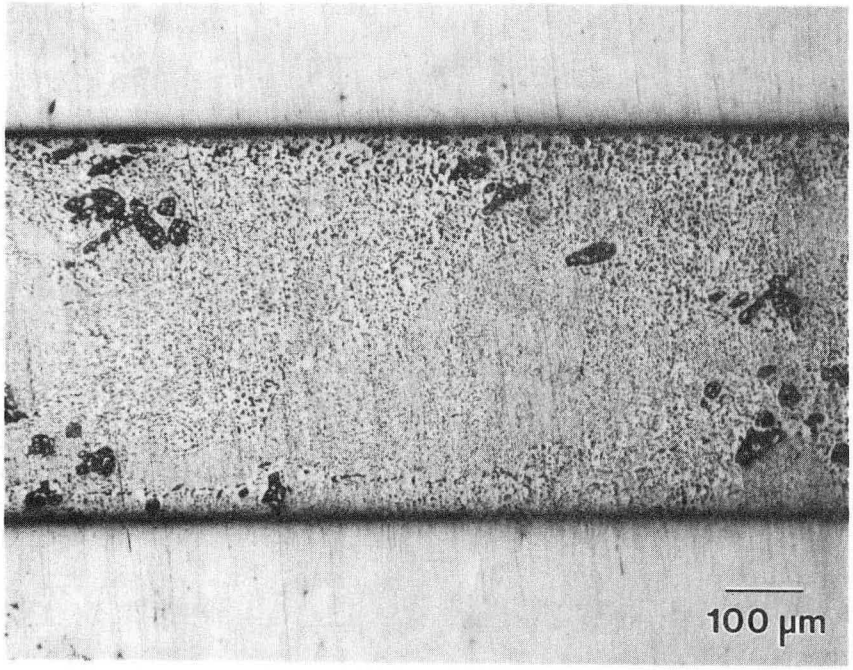

(b)

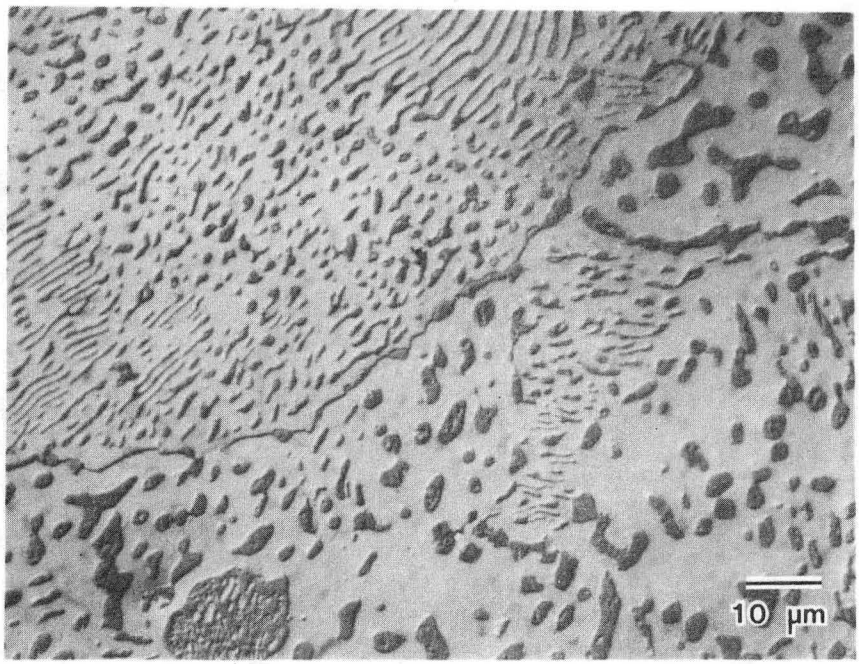

XBB 885-5425

Figure 22: Optical micrographs of the crack profile of the 60Sn-40Pb shear specimen.

(a)

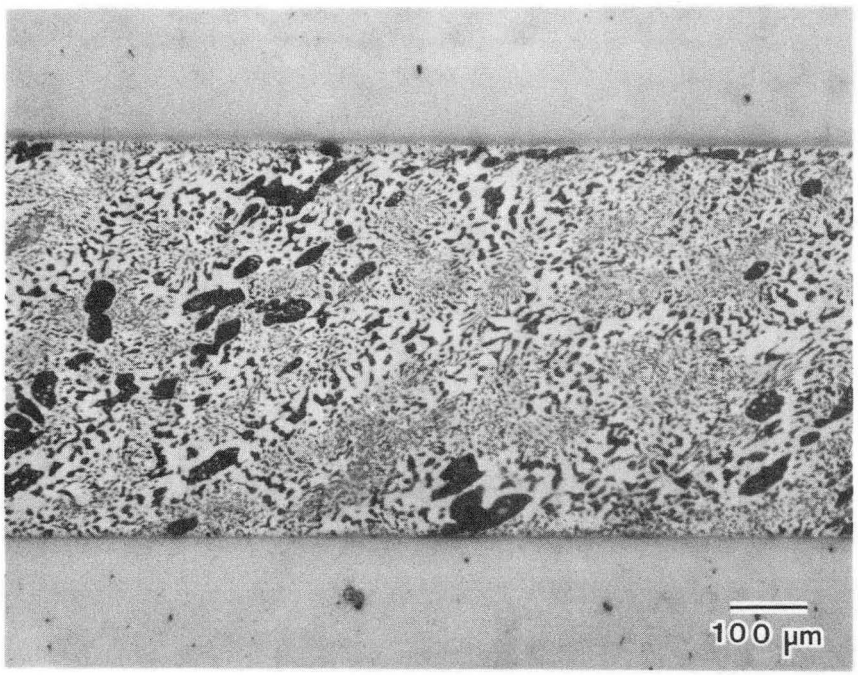

(b)

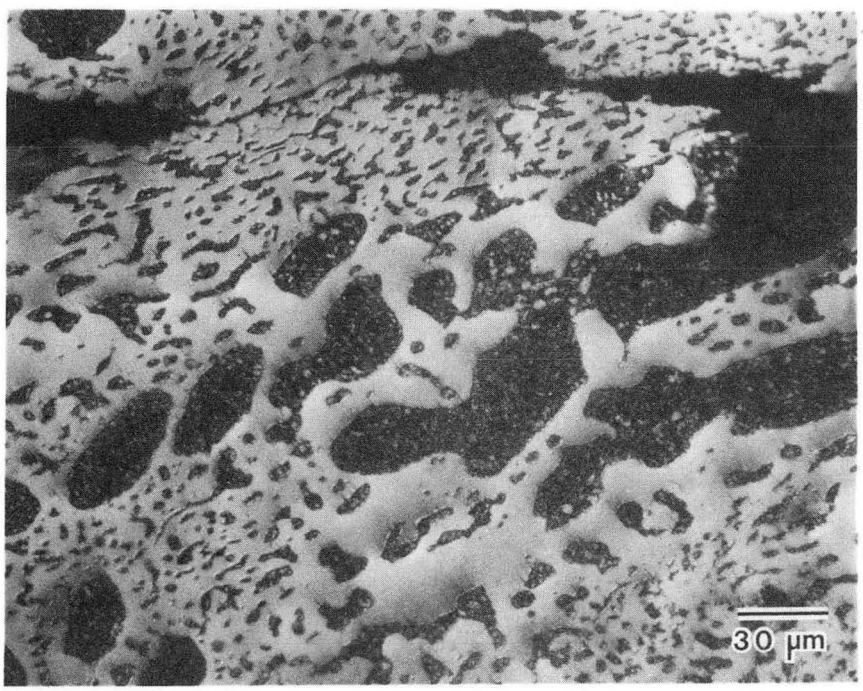

XBB 885-5426

Figure 23: Optical micrographs of the crack profile of the 58Sn-40Pb-2In shear specimen.

(a)

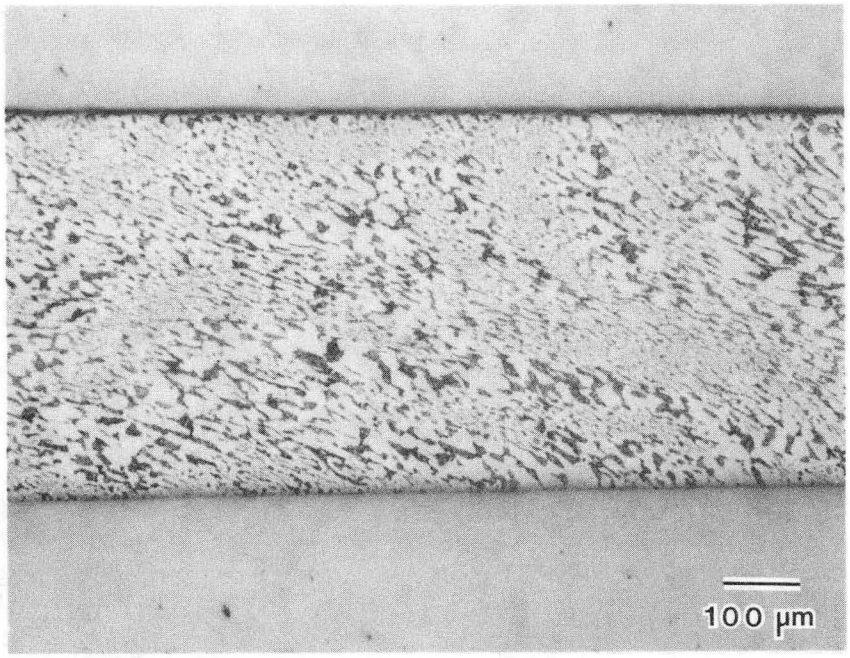

(b)

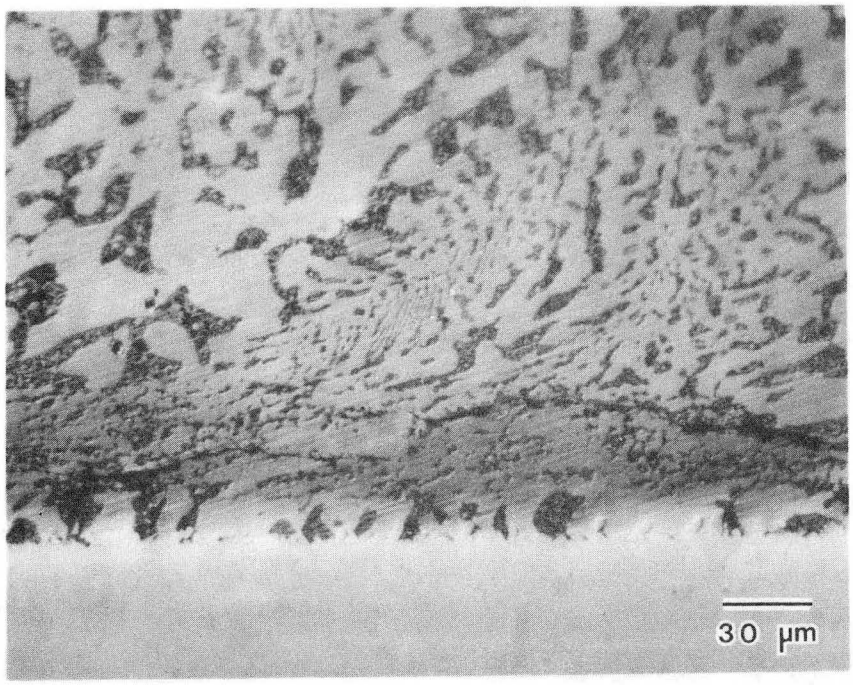

XBB 885-5427

Figure 24: Optical micrographs of the crack profile of the 58Sn-40Pb-2Bi shear specimen.

(a)

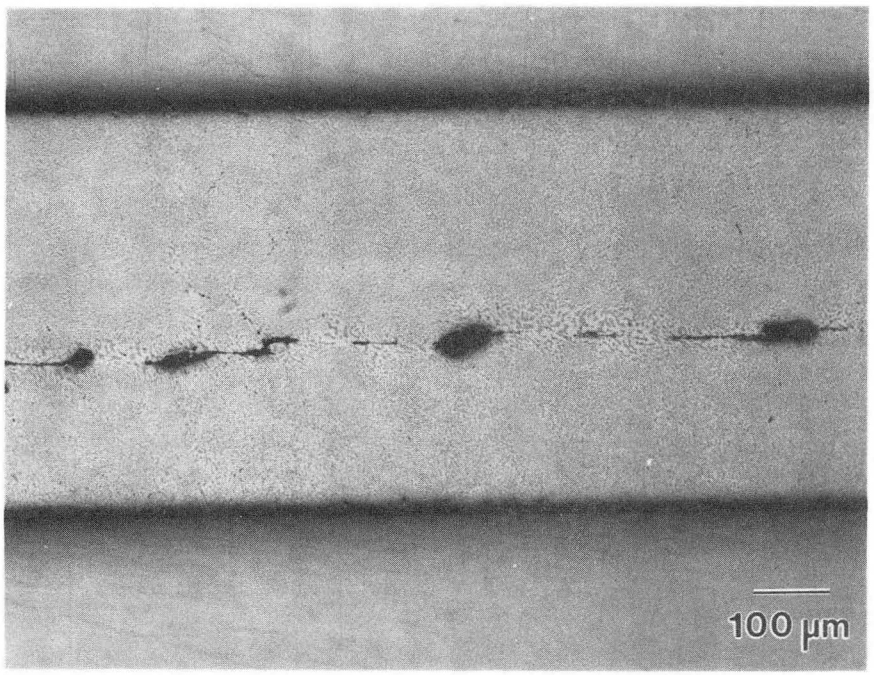

(b)

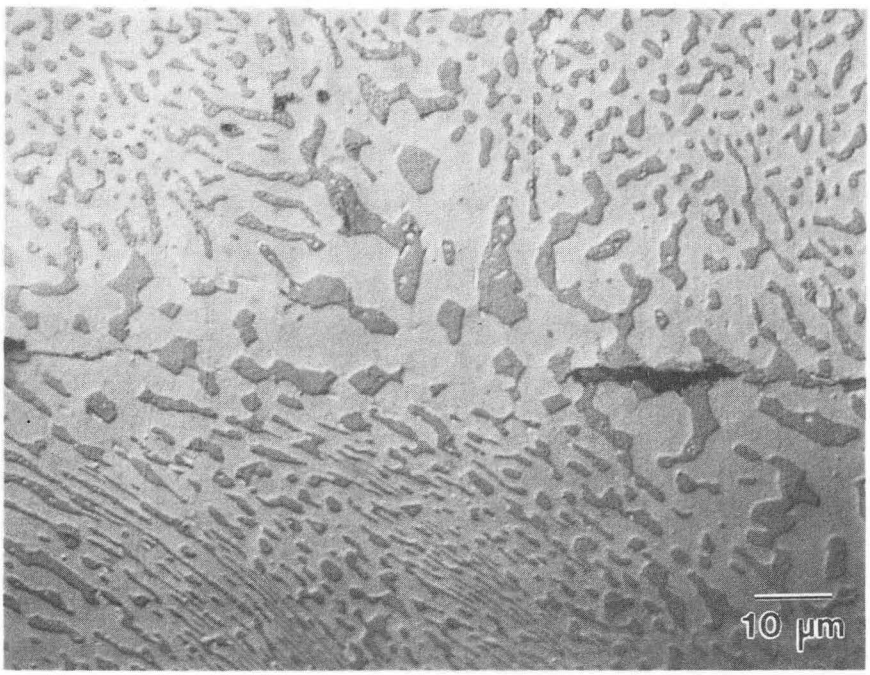

XBB 885-5428

Figure 25: Optical micrographs of the crack profile of the 58Sn-40Pb-2Sb shear specimen.

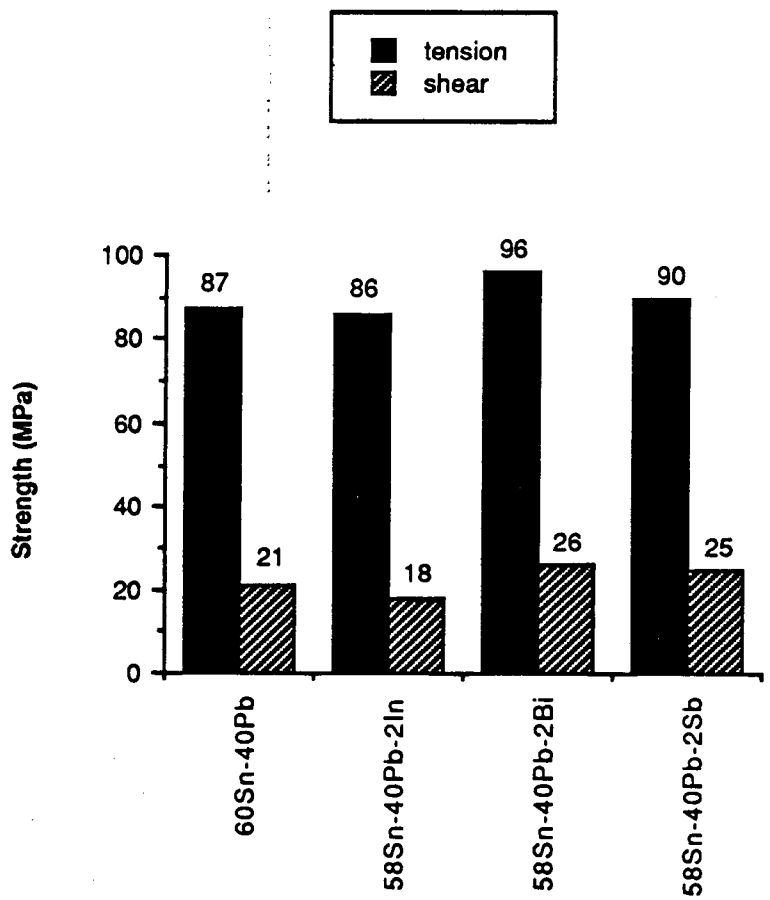

Figure 26: Bar graph of the tensile and shear strengths for all alloys tested.

phase particles - the individual particles of the separate phases

lamellar

globular

aligned globular

eutectic colonies - aggregates of phase particles in which the particles have some characteristic arrangement. Two eutectic colonies are shown at the right.

eutectic grains - the portion of the structure that nucleated at a certain site and/or in which the phase particles have definite crystallographic and metallographic relationships to one another. Three eutectic grains are shown in each of the following figures.

distinct grain boundaries

diffuse grain boundaries

Figure 27: Schematic representations of the characteristic features of eutectic structures.

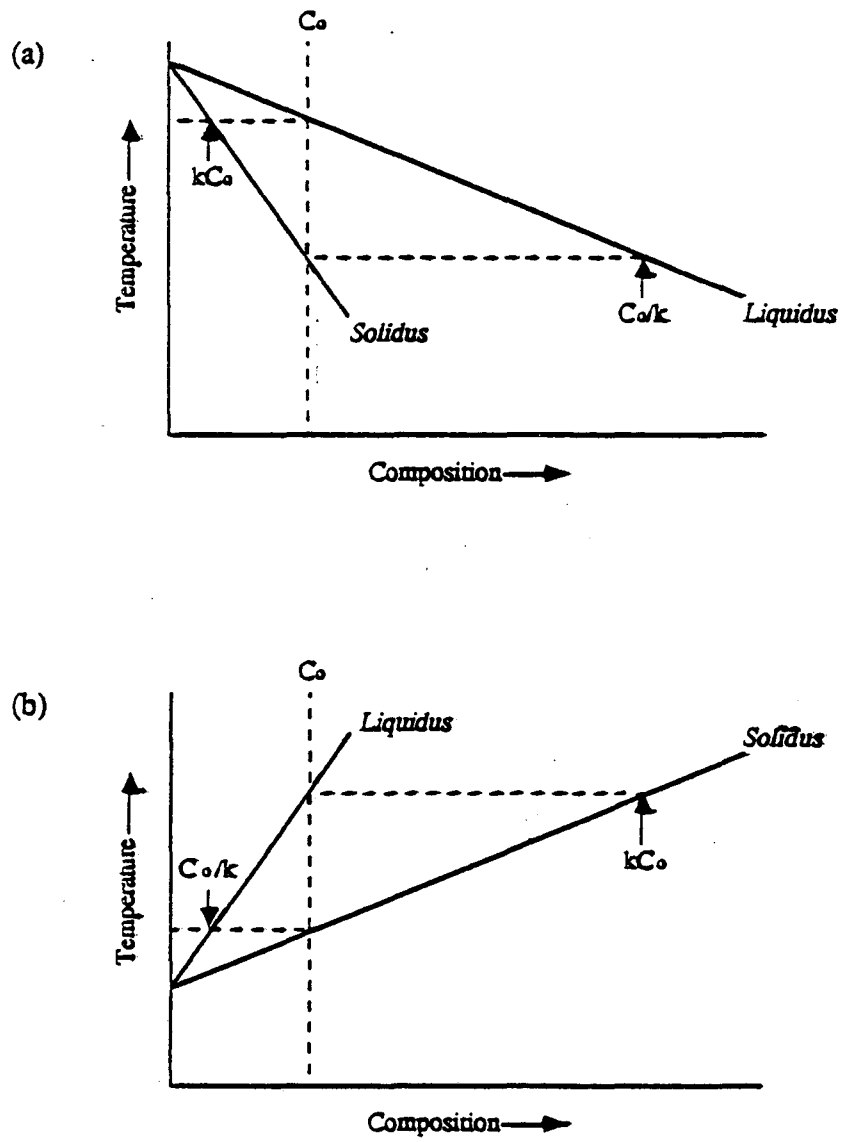

Figure 28: Simplified phase diagram to model nonequilibrium solidification for a single phase binary alloy for (a) k<1 and (b) k>1.

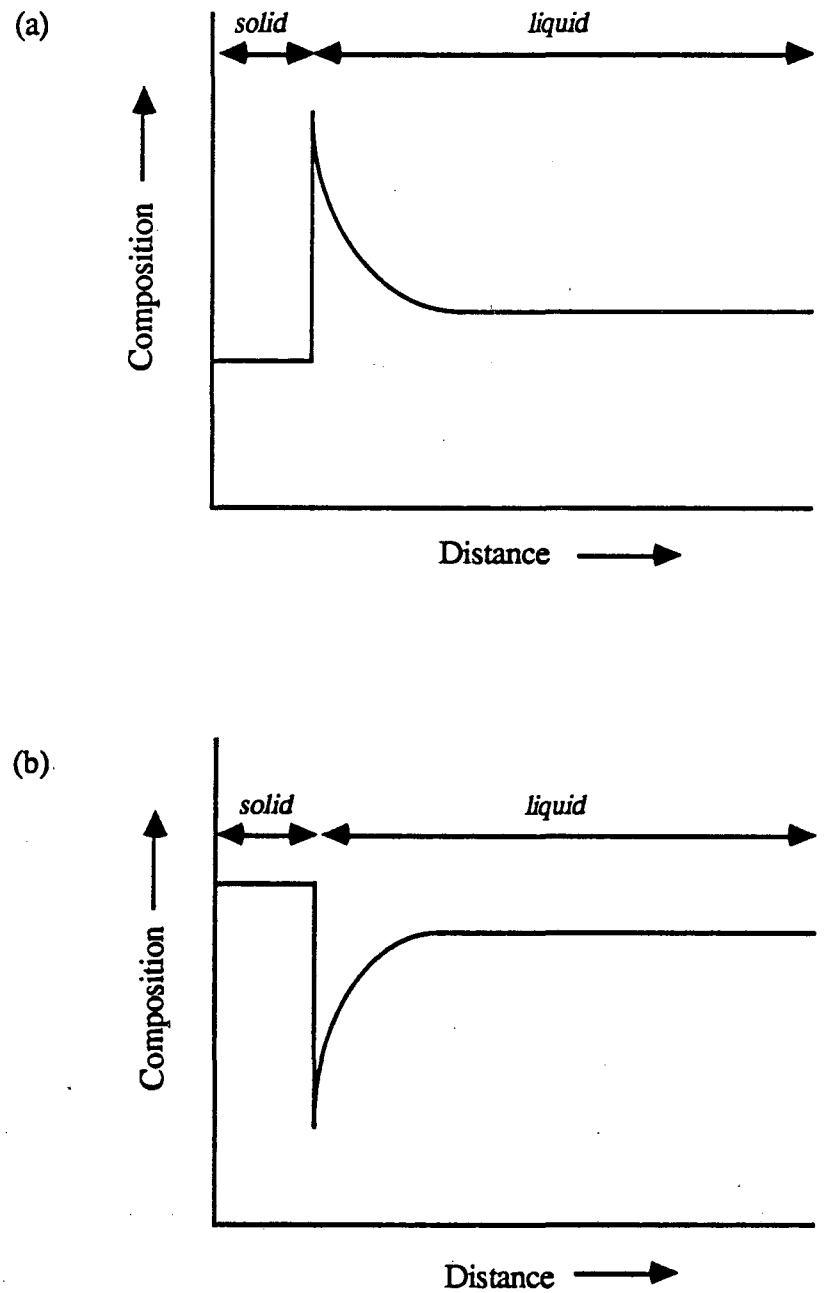

Figure 29: The concentration profile ahead of the solidification front for (a) k<1 and (b) k>1.

LAWRENCE BERKELEY LABORATORY
TECHNICAL INFORMATION DEPARTMENT
UNIVERSITY OF CALIFORNIA
BERKELEY, CALIFORNIA 94720